

# Hitting Multiple Cellular Targets in Triple-Negative Breast Cancer Using Dual-Action Cisplatin(IV) Prodrugs for Safer Synergistic Chemotherapy

Tushar Date, Kaushik Kuche, Dasharath Chaudhari, Rohan Ghadi, Deepak Kumar Sahel, Deepak Chitkara, and Sanyog Jain\*



Cite This: <https://doi.org/10.1021/acsbiomaterials.1c01582>



Read Online

ACCESS |



Metrics & More



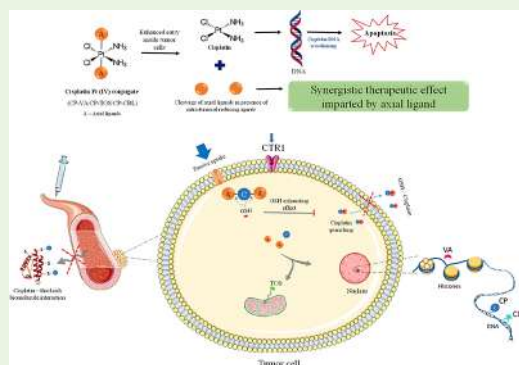
Article Recommendations



Supporting Information

**ABSTRACT:** Triple-negative breast cancer (TNBC) cells show improved sensitivity for cisplatin therapy due to their defective DNA damage repair system. However, the clinical utilization of cisplatin is limited by dose-dependent systemic toxicities and chemoresistance. Cisplatin Pt(IV) derivatives having kinetically inert octahedral geometry provide an effective strategy to overcome these limitations. Upon cellular reduction, these derivatives release cisplatin and axial ligands, acting as dual-action prodrugs. Hereby, we have developed three cisplatin(IV) conjugates using distinct bioactive axial moieties (valproate, tocopherol, and chlorambucil), which can synergistically complement cisplatin activity and attack multiple cellular targets. The designed derivatives showcased enhanced antiproliferative activity and improved therapeutic synergism along with a noteworthy cisplatin dose reduction index in a panel of six cancer cells. These Pt(IV) derivatives remarkably improved cellular drug uptake and showed lower dependency on copper transporter 1 (Ctr1) for uptake than cisplatin. The results of enhanced in vitro activity were well corroborated by in vivo efficacy testing in the 4T1 cell-based TNBC model, showcasing ~2–7-folds higher tumor volume reduction for Pt(IV) derivatives than cisplatin. In addition, the designed derivatives significantly reduced the nephrotoxicity risk involved in cisplatin therapy, indicated by systemic toxicity biomarkers and organ histopathology. The results indicated that cisplatin(IV) derivatives could open new avenues for safer synergistic chemotherapy in TNBC.

**KEYWORDS:** platinum(IV) prodrugs, breast cancer, cisplatin, drug delivery, nephrotoxicity



## 1. INTRODUCTION

Triple-negative breast cancer (TNBC) is one of the subtypes of aggressive mammary cancer characterized by the presence of invasive tumors having high proliferation and metastasis rate, increased recurrence, poor patient survival, and rapid chemoresistance development.<sup>1</sup> Ineffectiveness of endocrinal therapy and availability of limited treatment options make TNBC management challenging.<sup>2</sup> Breast cancer gene dysfunction in TNBC results in a defective DNA damage repair system, making TNBC cells highly sensitive to DNA-damaging drugs such as platinum (Pt) agents.<sup>3</sup> Notably, Pt therapy was found to be clinically effective in improving the response rate, pathological complete response rate, and patient survival in both early stages as well as advanced TNBC.<sup>4–6</sup> Cisplatin is a first-generation Pt anticancer agent and is often used as a key therapeutic option for TNBC management. Cell death induced by cisplatin is a multifaceted event involving interlinks between apoptosis, ferroptosis, and immunomodulatory pathways.<sup>7,8</sup> It primarily acts through DNA cross-linking followed by inhibition of DNA transcription and replication, leading to

apoptosis. Additionally, cisplatin induces cell death by modulating interplay between cellular events such as the generation of reactive oxygen species (ROS), altering cellular calcium homeostasis, triggering ferroptosis pathways, and activating death receptor signaling and mitochondrial apoptosis pathways.<sup>9</sup> Recently, cisplatin is also found to act as a potent immunomodulator for both innate and adaptive immunity by triggering upregulation of MHC class I expression, downregulating immunosuppression, and triggering proliferation of effector cells.<sup>10</sup>

Despite the strong immuno–chemotherapeutic activity, the clinical applicability of cisplatin in TNBC is severely limited by chemoresistance and systemic toxicities. Therapeutic efficacy

**Received:** December 18, 2021

**Accepted:** April 25, 2022



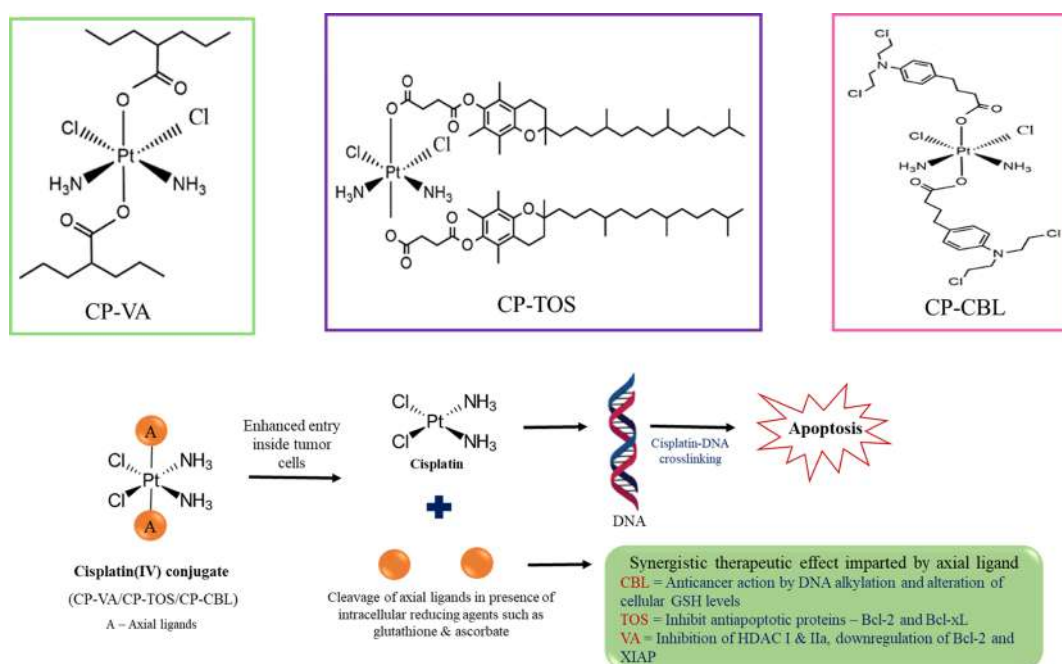


**Figure 1.** Graphical illustration of the chemical structures of developed cisplatin(IV) conjugates, their mechanism of intracellular reduction, and their subcellular targets for synergistic therapeutic action.

of cisplatin is restricted by severe dose-dependent systemic toxicities such as nephrotoxicity, ototoxicity, neurotoxicity, and emetogenesis. The rapid development of intrinsic and acquired cisplatin resistance results in ineffective platinum therapy.<sup>11,12</sup> More recently, cisplatin resistance has been reported even in TNBC despite its higher sensitivity toward cisplatin therapy.<sup>13</sup> In addition, due to the high kinetic reactivity of the cisplatin's structure, it shows strong off-target interactions with non-DNA molecules resulting in nonspecific biodistribution and systemic toxicities. The poor lipophilicity of cisplatin results in restricted cellular drug uptake and limits the effective drug concentration available at the tumor site. Therefore, overall shortcomings often limit the broad scale clinical utilization of cisplatin for TNBC treatment.

Designing cisplatin(IV) agents is an effective strategy to resolve the mentioned challenges and improve the effectiveness of cisplatin therapy in TNBC. Pt(IV) agents have low-spin d<sup>6</sup> Pt(IV) centers where the central Pt atom is conjugated with additional axial ligands. Unlike the square planar structure of cisplatin, its Pt(IV) derivatives are octahedral with six coordinates, making them saturated and kinetically more inert toward ligand substitution reactions, therefore minimizing unwanted interactions with non-DNA extracellular biomolecules and reducing the extent of Pt deactivation en route to tumor cells. Additionally, the presence of two axial ligands in the Pt(IV) structure provides an opportunity to enhance anticancer activity and fine-tune the lipophilicity of Pt(IV) conjugates to attain improved cellular uptake. Due to their d<sup>6</sup> electronic configuration, cisplatin Pt(IV) agents are stable outside the cancer cells, and after cellular entry, they undergo a reduction in the presence of intratumoral reducing agents [glutathione (GSH), ascorbate, metallothioneine, etc.] through electron reductive elimination to release cisplatin and axial ligands.<sup>14</sup> Therefore, the inclusion of bioactive axial ligands in the Pt(IV) structure can result in dual-action prodrugs or bi-pills where cisplatin and axial ligands can individually act on their pharmacological targets and attack

multiple biological pathways of tumor progression. Additionally, this strategy provides an opportunity to simultaneously deliver two chemotherapeutic agents in a predefined combination ratio to achieve synergistic tumor-targeted chemotherapy, which is not possible with conventional combination therapy.<sup>14,15</sup>

There has been significant research thrust in the field of Pt(IV) agents over the past decade, and many novel cisplatin(IV) derivatives were reported.<sup>15–18</sup> However, to date, very few reports explored the therapeutic potential of cisplatin(IV) derivatives in TNBC treatment. Considering factors such as current unavailability of standard treatment options for TNBC management, promising clinical response of cisplatin therapy in TNBC, and the effectiveness of Pt(IV) prodrug approach to improve the therapeutic benefits of cisplatin therapy, use of cisplatin(IV) agents could revolutionize the TNBC treatment paradigms. In this work, we have explored these untapped horizons by studying the effectiveness of three cisplatin(IV) prodrugs in TNBC treatment. These cisplatin(IV) conjugates were developed using distinct bioactive axial ligands; valproic acid (VA), D- $\alpha$ -tocopherol succinate (TOS), and chlorambucil (CBL). Axial ligands were selected based on their ability to synergistically complement the DNA damaging action of cisplatin as well as their bioactivity profile considering critical molecular pathways in the TNBC progression.<sup>19–21</sup> In the present work, we tried to explore the effectiveness of designed cisplatin(IV) compounds in TNBC treatment compared to cisplatin.

Designed Pt(IV) conjugates are referred as cisplatin-valproate (CP-VA), cisplatin-tocopherol (CP-TOS), and cisplatin-chlorambucil (CP-CBL) in this article. VA is an established histone deacetylase inhibitor (HDACi) and inhibits HDAC I and IIa.<sup>22</sup> Cisplatin majorly acts on nuclear DNA which exists as a highly condensed structure in association with histones, making cisplatin–DNA interaction critical barrier to attain therapeutic effect (only 1% of cellular Pt can interact with DNA).<sup>23</sup> HDAC inhibition leads to hyperacetylation of

DNA-associated histones and makes DNA more accessible for damage by Pt agents. Additionally, VA showcases supplementary anticancer activity and assists in downregulation of Bcl-2 and XIAP which play a key role in cisplatin chemoresistance development. TOS is a vitamin E analogue and presents potent anticancer activity by inhibiting antiapoptotic proteins, Bcl-2 and Bcl-xL, thereby triggering mitochondrial apoptosis pathway for cell death.<sup>24,25</sup> Notably, TOS treatment effectively triggered apoptosis in TNBC cells through the mitochondrial pathway.<sup>26</sup> Therefore, CP-TOS was designed to act as dual-action therapeutic by attacking DNA and mitochondria simultaneously. CBL is a clinically approved anticancer drug that acts as a DNA alkylator by binding to N3 of adenine and N7 of guanine or adenine bases in DNA and inhibits DNA replication resulting in cell death.<sup>27</sup> Additionally, it can alter cellular GSH level by catalyzing enzymatic activity of GSH S-transferase.<sup>28</sup> Therefore, TNBC treatment using CP-CBL could result in repair-resistant hybrid DNA damage through a combination of DNA alkylation and cross-linking, which could be difficult to be rectified by DNA repair machinery. Dual DNA damaging potential and cellular GSH modulation offered by CP-CBL can provide an effective chemo-redox strategy to treat TNBC. Developed cisplatin(IV) agents were envisioned to unleash a multilevel attack on the cellular pathways of TNBC progression and display enhanced anticancer activity, improved cellular drug uptake, and reduced risk of systemic side effects (Figure 1).

## 2. MATERIALS

Cisplatin was generously provided for research purpose by Neon Laboratories Ltd, India. Hydrogen peroxide, pyridine, TOS, magnesium chloride, di-*tert*-butyl dicarbonate (BOC anhydride), valproyl chloride, CBL, triethylamine, O-(benzotriazol-1-yl)-*N,N,N',N'*-tetramethyluronium tetrafluoroborate (TBTU), 2',7'-dichlorofluorescein diacetate (DCFH-DA), caspase-3 substrate (*N*-Acetyl-Asp-Glu-Val-Asp-7-amido-4-methylcoumarin), anhydrous *N,N*-dimethylformamide (DMF), and sulphorhodamine B sodium salt were purchased from Sigma-Aldrich, USA. Hoechst 33342 was purchased from Thermo Fisher Scientific, USA. Solvents such as acetone, diethyl ether, ethanol, dimethyl sulfoxide, hexane, tetrahydrofuran (THF), and ethyl acetate were procured from Merck, India. Dulbecco's modified Eagle medium (DMEM), fetal bovine serum, and all accessories related to cell culture studies were procured from Sigma-Aldrich, USA. Toxicity biomarker assay kits were purchased from AccuRex Biomedical Pvt. Ltd, India. All remaining reagents and chemicals utilized were purchased from local suppliers.

## 3. METHODS

### 3.1. Synthesis of Dual-Action Cisplatin(IV) Prodrugs.

**3.1.1. Synthesis of CP-VA.** Cis,cis,trans-[PtCl<sub>2</sub>(OH)<sub>2</sub>(NH<sub>3</sub>)<sub>2</sub>], referred as oxoplatin hereafter, was synthesized using a previously established method.<sup>29</sup> In brief, 20 mL of 30% w/v H<sub>2</sub>O<sub>2</sub> was added dropwise into aqueous cisplatin suspension (0.4 g cisplatin/10 mL water) maintained at 60 °C and stirred for 6 h protected from light. The product was cooled at room temperature and recrystallized at 4 °C overnight. The crystals were sequentially washed with ice-cold water, ethanol, and diethyl ether and dried to get bright yellow crystals of oxoplatin (yield—66.4%). For synthesis of CP-VA, the mixture of oxoplatin (200 mg, 0.3 mmol) and pyridine (2 mL, 12.4 mmol) in anhydrous acetone was dropwise added into acetone solution containing valproyl chloride (2.54 g, 7.8 mmol). The reaction mixture was refluxed under stirring in the dark for 14 h. After cooling at room temperature, the reaction mixture was dissolved in hexane (25 mL) followed by filtration, and the filtrate was concentrated using a rotaevaporator (Buchi, Switzerland). Ice-cold diethyl ether was added to the concentrate to get yellowish-white precipitate which was

filtered out and further washed with water. The product was washed with excess diethyl ether and dried under vacuum (yield—45.6%).

**3.1.2. Synthesis of CP-TOS.** First, TOS anhydride was synthesized using the reported protocol.<sup>30</sup> Briefly, the mixture of TOS (265 mg, 1 mmol), magnesium chloride hexahydrate (20.3 mg, 0.1 mmol), and BOC anhydride (275 mg, 2.5 mmol) was dissolved in 5 mL of anhydrous THF and stirred at 50 °C under nitrogen for 24 h. The reaction mixture was diluted with 10 mL of water and quickly extracted with ethyl acetate (10 mL × 3 times). The organic layer was separated, dried over sodium sulphate, and further concentrated using a rotaevaporator to get TOS anhydride in the form of viscous liquid. For CP-TOS synthesis, oxoplatin (81 mg, 0.48 mmol) and TOS anhydride (1 g, 1.94 mmol) were dissolved in anhydrous DMF and kept under stirring at 60 °C for 14 h. Excess ice-cold water (50 mL) was added to the reaction mixture followed by quick extraction with ethyl acetate (20 mL × 3 times). Aqueous fraction remained was again extracted with diethyl ether (20 mL × 3 times). Finally, ethyl acetate and diethyl ether fractions were mixed, dried over sodium sulphate, and concentrated using a rotaevaporator. At the end, 20 mL of ice-cold methanol was added to concentrate and stored at −20 °C overnight to get a yellowish viscous precipitate which was further dried under vacuum (yield—68.4%).

**3.1.3. Synthesis of CP-CBL.** A mixture of CBL (53 mg, 0.35 mmol), triethylamine (25 μL, 0.35 mmol), and TBTU (56 mg, 0.35 mmol) was added into the suspension of oxoplatin in anhydrous DMF (2 mL). The reaction mixture was stirred under nitrogen at 40 °C for 24 h. The reaction mixture was added into 10 mL of ice-cold water to get a dark red precipitate which was further washed with methanol and acetonitrile and dried in a vacuum oven (yield—46%).

The cisplatin: axial ligand ratio in all conjugates was 1:2. All synthesized conjugates were dialyzed for 12 h against water + DMF mixture followed by 12 h dialysis against water to ensure purity and removal of solvent traces (dialysis membrane cut-off—500 & 1000 Da, as required). The conjugates were further lyophilized and stored for further studies.

**3.2. Characterization.** Structural characterization of CP-VA, CP-TOS, and CP-CBL conjugates was carried out using <sup>1</sup>H and <sup>13</sup>C NMR, mass spectroscopies, and these details could be referred in the Supporting Information.

**3.3. Cell Culture Studies.** **3.3.1. MTT Assay.** Antiproliferative effect of cisplatin(IV) conjugates was tested in various carcinoma cell lines in comparison with established Pt drugs as well as equimolar physical mixtures (1:2 mol) of cisplatin with respective axial ligands using the MTT assay. For the study, A549 (human lung carcinoma), SKOV-3 (human ovarian adenocarcinoma), MCF-7 (human breast carcinoma), MDA-MB 231 (human breast carcinoma—TNBC variant), HeLa (human cervical adenocarcinoma), and U87 (human glioblastoma) cells were seeded into a 96-well plate. All cells were grown in DMEM cell culture medium and were exposed to suitable concentrations of test compound for 24 h. Afterward, the media was aspirated, and the cells were washed with phosphate-buffered saline (PBS) and added to 200 μL of 3-(4,5-dimethylthiazol-2-yl)-2,5-diphenyltetrazolium bromide (MTT) reagent to estimate the antiproliferative activity of test compounds using an enzyme-linked immunosorbent assay (ELISA) plate reader at 540 nm (BioTek, USA). The cell viability was calculated by the following equation: % cell viability = test group absorbance/control group absorbance × 100. IC<sub>50</sub> values for each test group was calculated using CompuSyn software.

**3.3.2. Sulphorhodamine B Assay.** The sulphorhodamine B assay was performed in MDA-MB-231 cells to validate the findings from the MTT assay. The percent cell viability was determined by the sulphorhodamine B assay as per a previously published report.<sup>31,32</sup> In brief, the cells were seeded in a 96-well flat-bottom tissue-culture plate at 2 × 10<sup>4</sup> cells/well density. Immediately, the cells were exposed to suitable concentrations of test groups and were incubated under humidified 5% CO<sub>2</sub> atmosphere at 37 °C for 24 h. To each well, 25 μL of cold 50% (w/v) trichloroacetic acid was gently added and incubated for 1 h at 4 °C. The plates were washed four times with water and air-dried at room temperature. Next, 50 μL of 0.04% (w/v)



of sulphorhodamine B sodium salt in 1% (v/v) of acetic acid was added to each well and incubated for 1 h at room temperature. Immediately after the incubation, the wells were rinsed with 1% (v/v) acetic acid to remove the unbound dye and air-dried at room temperature. Finally, 100  $\mu\text{L}$  of 10 mM Tris base solution (pH 10.5) was added to each well for solubilizing the protein bound dye. The absorbance was measured at 510 nm using a UV plate reader (BioTek, USA). Percent cell viability was measured using the following formula: % cell viability = absorbance of sample/absorbance of control  $\times$  100. IC<sub>50</sub> value for each test group was calculated using CompuSyn software.

**3.3.3. Estimation of Therapeutic Synergy and Dose Reduction Potential of Cisplatin Conjugates.** Synergistic activity and dose reduction potential of synthesized cisplatin(IV) conjugates and their physical mixtures were analyzed from the MTT assay-based cell viability data by calculating the combination index (CI) and dose reduction index (DRI) using CompuSyn software. The CI values were used to predict the extent of synergy for cisplatin conjugates [additive effect (CI = 1), synergism (CI < 1), and antagonism (CI > 1)], while the DRI value provided an estimate of how many folds the dose of each drug in a synergistic combination may be reduced compared with the individual doses of each drug alone.<sup>33,34</sup>

**3.3.4. Cellular Drug Uptake.** MDA-MB-231 cells were seeded at  $1 \times 10^6$  cell/well density in a 6-well plate. After 24 h incubation, cells were exposed to 5  $\mu\text{M}$  concentration of cisplatin, CP-VA, CP-TOS, CP-CBL, and respective physical mixtures of cisplatin with axial ligands (1:2 mol) for 6 h at 37  $^\circ\text{C}$ . Suitable precautions in experimental conditions were taken to ensure that maximum (>95%) cells were alive during the uptake experiment. Post incubation, the cells were washed thrice with PBS to remove excess drug and were digested using 500  $\mu\text{L}$  of 67–69% nitric acid (Suprapur, Merck, USA) for 4 h at 60  $^\circ\text{C}$ . Subsequently, 400  $\mu\text{L}$  of digested cell lysate was diluted with 9.6 mL of distilled deionized water, and the Pt content in the sample was determined using ICP–MS (Agilent 7700 ICP–MS, Japan). Additionally, cellular uptake in presence of copper transporter 1 (Ctr1) inhibitor was carried out to understand the impact of Pt(IV) prodrug formation on the extent of cellular drug internalization. For this, cellular uptake analysis was carried out in the presence of Ctr1 inhibitor (copper sulfate—1 mM, used as competitive Ctr1 inhibitor) using the above-mentioned protocol.

**3.3.5. GSH Assay.** Total cellular GSH level after treatment with synthesized Pt(IV) conjugates was analyzed using the GSH assay kit (Clontech, Mountain view, USA). MDA-MB-231 cells ( $4 \times 10^6$  cells/well) were treated with 5  $\mu\text{M}$  test groups for 24 h. Post treatment, the cells were washed thrice with PBS and trypsinized, and cell pellets were obtained by centrifugation (1500 rpm, 5 min). Subsequently, the cells were lysed using lysis buffer [10 mM Tris–HCl, 320 mM sucrose, 1% Triton X-100, 5 mM ethylenediaminetetraacetic acid, and 2 mM 1,4-dithio-DL-threitol buffer; pH 7.6] for 15 min in ice bath, and the cell lysate was separated by centrifugation (15 000 rpm, 20 min at 4  $^\circ\text{C}$ ). The supernatant from cell lysate of each test group was added to the monochlorobimane dye (2  $\mu\text{L}$ , 100 mM concentration) to attain a final concentration of 2 mM for each test group. Monochlorobimane is a thiol-sensitive dye which gets converted into a blue fluorescent derivative in the presence of GSH. The fluorescent intensity of each test solution was measured at  $\lambda_{\text{excitation}} = 395$  nm and  $\lambda_{\text{emission}} = 480$  nm using a spectrofluorometer.

**3.3.6. ROS Production.** Cisplatin and its derivatives are well reported to induce ROS generation which further triggers cell death pathways. To understand intracellular ROS-inducing potential for cisplatin conjugates, MDA-MB-231 cells ( $1 \times 10^6$  cells/well) were treated with 5  $\mu\text{M}$  of each test group for 6 h followed by washing with PBS. Fresh media containing 20  $\mu\text{M}$  DCFH-DA dye was added to each well and incubated for additional 1 h. To ensure uniformity of the experiment, all wells were seeded with cells of the same passage number and were seeded from the same cell suspension prepared from the same cultured T75 flask. Qualitative estimate of intracellular ROS generation after drug treatment was analyzed through relative

fluorescent intensity using confocal laser scanning microscopy (CLSM, Olympus FV1000, USA).

**3.3.7. Apoptosis Assay.** MDA-MB-231 cells were seeded in a 6-well cell culture plate ( $1 \times 10^6$  cells/well). After 24 h incubation, the cells were exposed to test groups (5  $\mu\text{M}$  each) for 48 h followed by washing with PBS (pH 7.4). Finally, the cells were trypsinized, separated by centrifugation (1500 rpm, 5 min), and resuspended in 1X annexin binding buffer. The cells were stained using FITC-tagged Annexin-V (ThermoFisher Scientific, USA) and propidium iodide, and cellular apoptosis was quantified using a flowcytometer (Cytotflex, Beckman Coulter, USA). Experimental data were analyzed with help of CytExpert version 2.0 software.

**3.3.8. Cell Cycle Analysis.** MDA-MB-231 cells ( $5 \times 10^6$  cells/well) were treated with individual test groups (5  $\mu\text{M}$  each) for 24 h. Post treatment, cells were washed with PBS, trypsinized, and separated by centrifugation (1500 rpm, 5 min). Cell pellets were resuspended in 1 mL of precooled 70 % v/v ethanol solution, followed by staining with propidium iodide at room temperature. Finally, cell cycle arrest analysis was carried out using a flowcytometer (Cytotflex, Beckman Coulter, USA), and data were analyzed through CytExpert software.

**3.3.9. Mitochondrial Membrane Potential Analysis.** MDA-MB-231 cells were seeded in a 96-well plate (80 000 cells/well). After overnight incubation, cells were treated with test groups—cisplatin, CP-VA, CP-TOS, CP-CBL (5  $\mu\text{M}$  each) and equimolar physical mixtures. After 24 h, the medium was replaced with fresh medium containing JC-1 (4  $\mu\text{g/mL}$ , Thermo Fisher Scientific, USA) and incubated for 30 min. Subsequently, the cells were washed thrice with PBS and analyzed under a plate reader using double excitation and emission at 485/528 and 530/590 nm. Mitochondrial depolarization of cells was indicated by the reduction in the red/green fluorescence intensity ratio, out of which, red fluorescence corresponds to potential-dependent JC-1 aggregation in mitochondria while green fluorescence corresponds to JC-1 monomers in cytosol.

**3.3.10. Intracellular  $\text{K}^+$  Leakage Estimation.** Leakage of  $\text{K}^+$  ions is closely linked with the initiation of apoptosis cascade. Therefore,  $\text{K}^+$  leakage after drug treatment was analyzed. For this study, MDA-MB-231 cells were exposed to 5  $\mu\text{M}$  cisplatin, CP-CBL, CP-TOS, and CP-VA along with the control group (no treatment) and incubated for 4 h. After every 1 h of incubation, the cell suspension sample was collected and centrifuged, and the supernatants were analyzed for extracellular  $\text{K}^+$  concentration using an ion-selective electrode (Orion Star, Thermo Scientific, Singapore). At the end, the cells were trypsinized, pelletized by centrifugation, resuspended in deionized water, and sonicated (2 min, 40 amplitude) to determine 100%  $\text{K}^+$  level. Percent  $\text{K}^+$  leakage at each time point was determined by the formula: %  $\text{K}^+$  leakage =  $([\text{K}^+] - [\text{K}^+]_0)/([\text{K}^+]_{\text{s}} - [\text{K}^+]_0) \times 100$ , where  $[\text{K}^+]$  corresponds to potassium leakage induced by the test compound and  $[\text{K}^+]_0$  and  $[\text{K}^+]_{\text{s}}$  are potassium leakage with no treatment (control) and after sonication, respectively.

**3.3.11. Studying Disruption of Cellular  $\text{Ca}^{2+}$  Homeostasis.** Mitochondrial  $\text{Ca}^{2+}$  uptake is closely associated with the activation of apoptotic factors such as caspases and cytochrome *c*. Therefore, analysis of  $\text{Ca}^{2+}$  level in cytosol and mitochondria was studied using cytosolic  $\text{Ca}^{2+}$ -specific reagent, Fura-2AM, and mitochondrial  $\text{Ca}^{2+}$ -specific reagent, Rhod-2AM (both from Thermo Fisher Scientific, USA). For the study, MDA-MB-231 cells ( $1 \times 10^6$  cells/well) were treated with 5  $\mu\text{M}$  cisplatin, CP-CBL, CP-TOS, and CP-VA for 4 h. Post incubation, the cells were washed thrice with Krebs buffer (calcium free), and cell suspensions were individually incubated with 10  $\mu\text{M}$  Rhod-2AM and 5  $\mu\text{M}$  Fura-2AM at 37  $^\circ\text{C}$  for 30 min. Cells were washed twice with Krebs buffer and fluorescent intensities of cell samples were measured using a spectrofluorometer (Rhod-2AM samples:  $\lambda_{\text{excitation}} = 550$  nm,  $\lambda_{\text{emission}} = 580$  nm; Fura-2AM samples:  $\lambda_{\text{excitation}} = 335$  nm,  $\lambda_{\text{emission}} = 505$  nm).

**3.3.12. Nuclear Staining.** MDA-MB-231 cells were grown in a 6-well plate ( $1 \times 10^6$  cells/well). After 24 h incubation, the cells were treated with 5  $\mu\text{M}$  of test groups for 24 h. At the end, the media was aspirated, and the cells were washed with PBS and fixed with 2% v/v glutaraldehyde solution for 10 min followed by washing with PBS. Cells were stained with 10  $\mu\text{g/mL}$  Hoechst 33 342 for 15 min

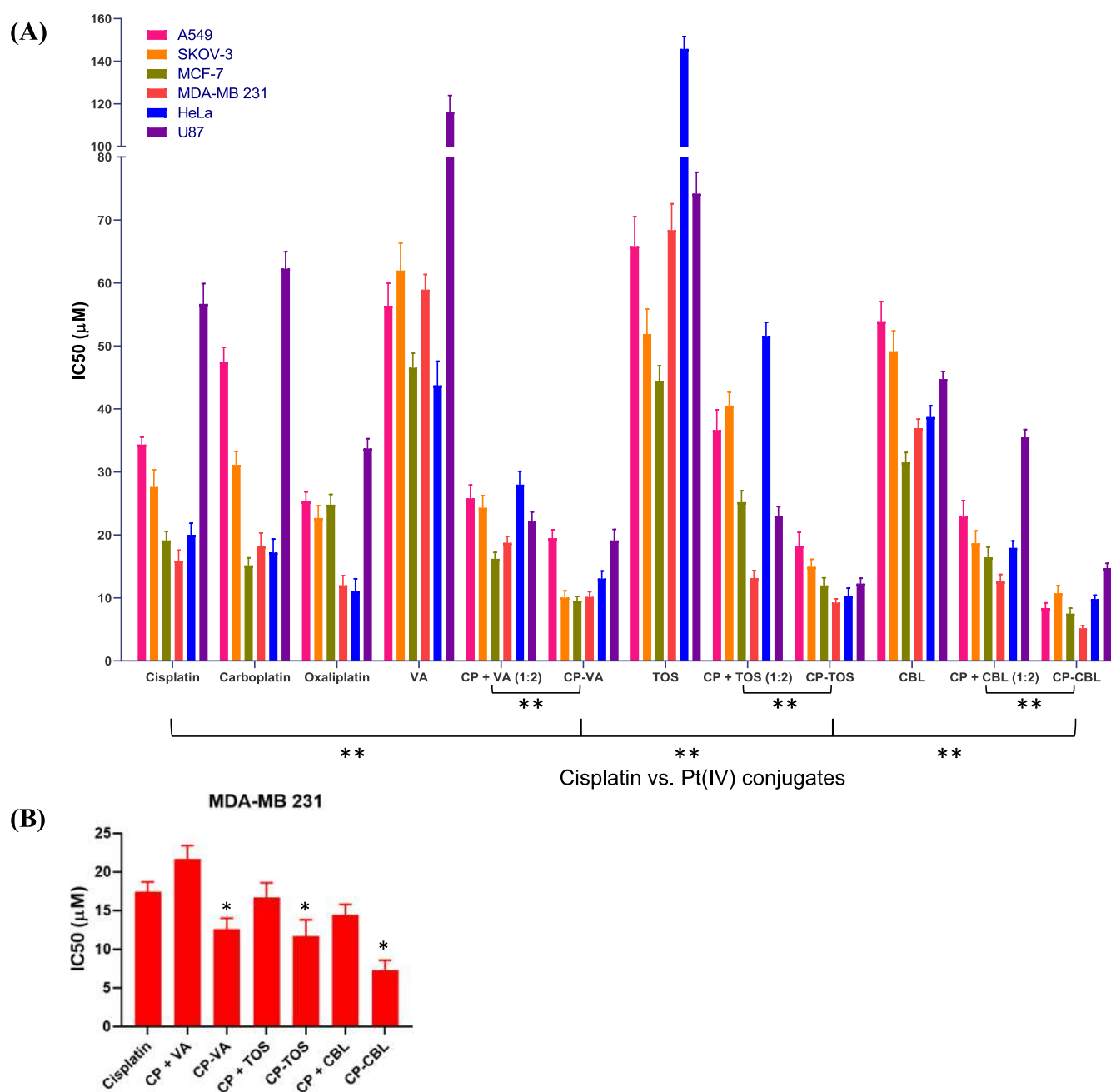


**Figure 2.** (A) IC<sub>50</sub> values obtained through MTT assay of marketed Pt drugs, axial ligands, cisplatin + axial ligand physical mixtures, and designed cisplatin(IV) conjugates in various cell lines; statistical significance (\*\* $p < 0.0001$ ) compared by two-way ANOVA. (B) IC<sub>50</sub> values obtained through sulphorhodamine B assay in MDA-MB 231 cells after treatment of cells with cisplatin, cisplatin + axial ligand physical mixtures, and designed cisplatin(IV) conjugates; statistical significance (\* $p < 0.001$ ) compared with the cisplatin group by two-way ANOVA.

protected from light. Cells were rewashed with PBS and observed using CLSM at  $\lambda_{\text{excitation}} = 405 \text{ nm}$  and  $\lambda_{\text{emission}} = 460 \text{ nm}$ .

**3.3.13. Caspase-3 Assay.** MDA-MB-231 cells ( $1 \times 10^6$  cells/well) were grown overnight and treated with doses equivalent to IC<sub>50</sub> of each test group for 24 h. Post treatment, the cells were washed twice with PBS, trypsinized, and pelleted by centrifugation. The harvested cells were homogenized on ice bath in lysis buffer using a probe sonicator (2 min, 40 amplitude). Protein aliquots for each test group (100  $\mu\text{L}$ ) were separated and exposed to caspase-3 substrate for 60 min at 37 °C in the dark. Interaction with cellular caspase-3 results in the hydrolysis of caspase-3 substrate to release the fluorescent derivative—7-amino-4-methylcoumarin. The fluorescent intensity of cell samples was measured using a spectrofluorometer to understand the levels of caspase-3 generated after drug treatment ( $\lambda_{\text{excitation}} = 380 \text{ nm}$ ;  $\lambda_{\text{emission}} = 460 \text{ nm}$ ).

**3.4. In Vivo Studies.** All in vivo experiments were performed in accordance with approved protocols (protocol number—IAEC/19/66-ext 1) from the Institutional Animal Ethics Committee (IAEC) of National Institute of Pharmaceutical Education and Research (NIPER), SAS Nagar, India. Institutional animal ethics guidelines were strictly followed during all stages of experimentation.

**3.4.1. Anticancer Efficacy Study.** Anticancer efficacy of dual-action Pt(IV) conjugates in TNBC was tested using the 4T1 cell line-induced tumor model in BALB/c mice. Tumors were induced in female BALB/c mice by subcutaneous injection of  $1 \times 10^5$  4T1 cells into the mammary fat pad. After uniform tumor growth (average tumor volume—200  $\text{mm}^3$ ), the animals were randomly divided into five groups each containing five animals. Animals were treated with cisplatin, CP-VA, CP-TOS, and CP-CBL at 8 mg/kg dose. Each group received four intravenous doses at interval of 7 days (dosing on

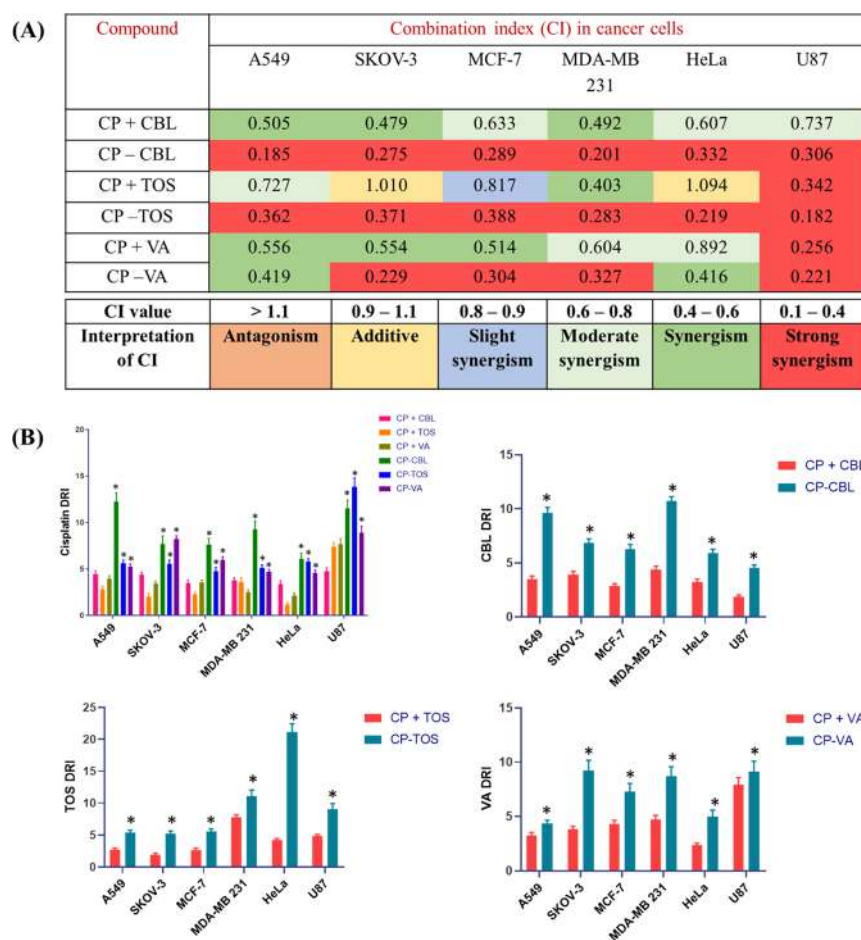


**Figure 3.** (A) CI values in various cancer cell lines after treatment with cisplatin + axial ligand physical mixtures and cisplatin(IV) conjugates as an indicator of the extent of therapeutic synergy. (B) DRI values for cisplatin and axial ligands in various cancer cell lines obtained after treatment with cisplatin + axial ligand physical mixtures and cisplatin(IV) conjugates; statistical significance ( $p < 0.05$ ) for cisplatin(IV) derivatives compared with the respective physical mixture group (cisplatin + axial ligand) by two-way ANOVA.

0, 7, 14, 21st day). During the study, the tumor volume and animal body weight of animals in each group were monitored at regular intervals. After completion of the study, the tumors were harvested, and anticancer efficacy of test groups was analyzed by calculating the tumor weight, tumor volume, tumor burden, and tumor inhibition rate, where tumor volume =  $\text{length} \times \text{width}^2/2$ ; % tumor inhibition rate =  $(W_c - W_t)/W_c \times 100$  ( $W_c$ —average tumor weight in control group and  $W_t$ —average tumor weight in test group); % tumor burden = average tumor weight/average body weight  $\times 100$ .

**3.4.2. Toxicity Analysis.** To evaluate the systemic toxicity induced by Pt(IV) conjugates, healthy Swiss albino mice (20–25 g) were randomly divided into five groups, each group containing five animals. Every group received 8 mg/kg intravenous dose of test groups four times at an interval of 7 days.

**3.4.2.1. Blood Biochemistry.** After completion of the study, blood samples were collected and analyzed for aspartate aminotransferase (AST), alanine aminotransferase (ALT), alkaline phosphatase (ALP), blood urea nitrogen (BUN), and creatinine levels using commercial diagnostic kits (AccuRex Biomedical Pvt. Ltd, India).

**3.4.2.2. Renal Damage Biomarkers.** To assess drug-induced kidney damage, kidneys were separated from treated animals, and whole kidney homogenate was prepared on ice bath in PBS using the tissue homogenizer (Polytron PT 4000, USA). The supernatant was separated by centrifugation and analyzed for kidney damage biomarkers—malondialdehyde (MDA), interleukin-6 (IL-6), and tumor necrosis factor- $\alpha$  (TNF- $\alpha$ ) using commercial ELISA kits as per manufacturer's protocol (AccuRex Biomedical Pvt. Ltd, India).

**3.4.2.3. Organ Histopathology.** Vital organs such as kidney, liver, spleen, lung, and heart were harvested from treated animals and

processed for hematoxylin and eosin (H&E) staining for organ histopathology analysis.

**3.5. Statistical Analysis.** Experimental data were analyzed for statistical significance using GraphPad Prism 8.0 software. Results with  $p \leq 0.05$  were considered as statistically significant.

## 4. RESULTS AND DISCUSSION

**4.1. Synthesis and Characterization.** Details of structural characterization for CP-VA, CP-TOS, and CP-CBL are provided in the [Supporting Information](#).

**4.2. Cell Culture Studies.** **4.2.1. MTT Assay.** The cell viability study was conducted through the MTT assay in a panel of human carcinoma cells and compared with cisplatin, next-generation Pt agents (carboplatin and oxaliplatin), and a physical mixture of cisplatin with respective axial moieties (1:2 mol ratio). The study was carried out to test the antiproliferative activity of synthesized cisplatin conjugates and compare their effectiveness against established Pt drugs. Preferential antiproliferative activity in cancerous cells was noted for developed conjugates in comparison with non-cancerous cells (refer the [Supporting Information](#) for antiproliferative study data in noncancerous cells). Concentration-dependent decrease in cell viability was noted in all test compounds. CP-VA, CP-TOS, and CP-CBL exhibited significantly improved antiproliferative activity and remarkably reduced  $IC_{50}$  values in all cell lines compared to marketed Pt



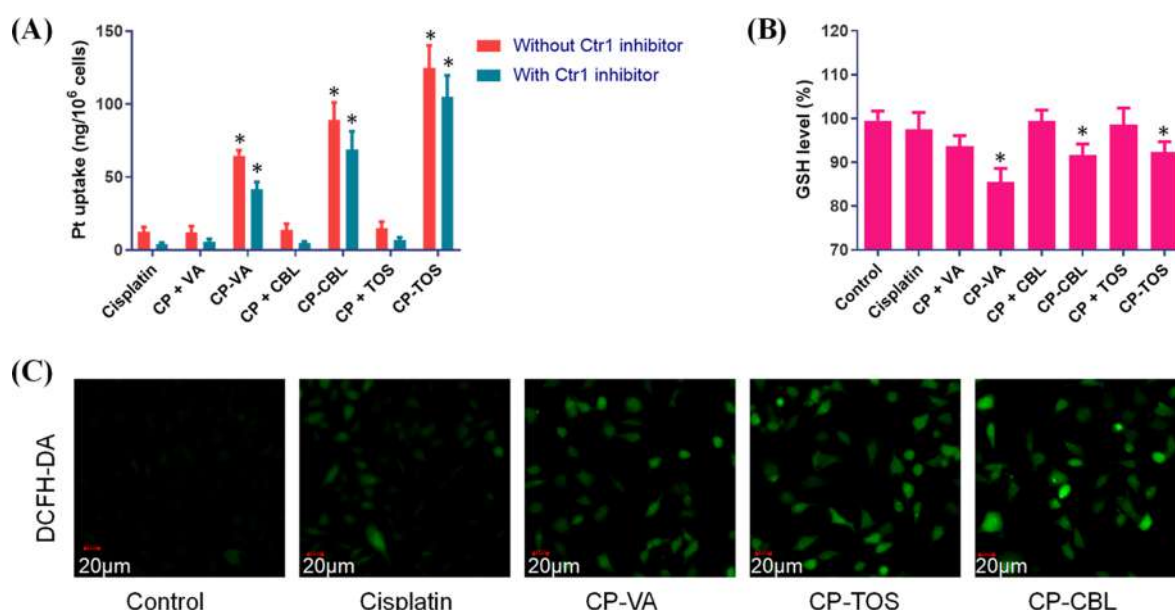


**Figure 4.** (A) Total Pt uptake in MDA-MB-231 cells after 6 h treatment with various test groups in the presence and absence of Ctr1 inhibitor (copper sulfate—1 mM); statistical significance (\* $p < 0.0001$ ) compared with cisplatin by two-way ANOVA. (B) Percent GSH level in MDA-MB-231 cells after 24 h treatment with various test groups; statistical significance (\* $p < 0.01$ ) compared with cisplatin by two-way ANOVA. (C) Intracellular ROS generation after treatment with test groups indicated by green fluorescence of DCFH-DA dye.

drugs as well as their respective physical mixtures (Figure 2A). Notable reduction in  $IC_{50}$  values for synthesized Pt(IV) derivatives indicated the prime role of Pt(IV) prodrug formation in improving the antiproliferative activity of cisplatin. Multidrug action imparted by cisplatin and axial ligands and improved lipophilicity of Pt(IV) conjugates (aiding in cellular drug uptake) could be the reason behind improved antiproliferative activity.<sup>35</sup> The  $IC_{50}$  values for all test compounds were lower in MDA-MB-231 compared to other cancer cell lines, indicating higher sensitivity of TNBC cells towards Pt-based chemotherapy.<sup>36,37</sup> CP-CBL displayed the lowest  $IC_{50}$  values in nearly all cancer cells compared to CP-VA and CP-TOS, which could be attributed to dual DNA damaging activity of cisplatin and CBL.

**4.2.2. Sulphorhodamine B Assay.** The sulphorhodamine B assay was performed in MDA-MB-231 cells to validate the findings from the MTT assay. The cell viability trend and the overall results from the sulphorhodamine assay were in-line with MTT assay results. In the sulphorhodamine assay, cisplatin(IV) conjugate-treated groups showed higher activity than cisplatin and cisplatin + axial ligand physical mixture-treated groups, denoting the role of Pt(IV) prodrug formation in enhancing cisplatin's activity. Out of the three cisplatin(IV) conjugates developed, CP-CBL showcased the highest activity, which could be explained through its dual-DNA damaging activity through the combined action of cisplatin and CBL (Figure 2B).

**4.2.3. Estimation of Therapeutic Synergy and Dose Reduction Potential of Cisplatin Conjugates.** Therapeutic synergy for CP-VA, CP-TOS, and CP-CBL was estimated in comparison with the physical mixtures of cisplatin with the respective axial ligand (1:2 mol ratio) using the Chou-Talalay method.<sup>33</sup> The CI values derived from CompuSyn software were used to predict the extent of synergy for Pt(IV) conjugates [additive effect (CI = 1), synergism (CI < 1), and antagonism (CI > 1)]. For synergy comparison, interpretation of CI values was further broken down as

shown in Figure 3A. Strong synergism (CI = 0.1–0.4) was noted for CP-CBL and CP-TOS in all cancer cell lines. The CI values for CP-VA, CP-TOS, and CP-CBL in all cell lines were markedly lower than their physical mixtures, highlighting enhanced therapeutic synergy for Pt(IV) conjugates than combination therapy. The DRI value provides an estimate of how many folds the dose of each drug in a synergistic combination may be reduced compared with the doses of individual drug alone. The dose reduction potential of CP-VA, CP-TOS, and CP-CBL was estimated using DRI analysis compared with individual drug therapy and combination therapy of cisplatin with respective axial ligands (Figure 3B). DRI analysis indicated that the synthesized Pt(IV) derivatives, that is, CP-VA, CP-TOS, and CP-CBL, resulted in higher extent (~2–5 folds) of cisplatin dose reduction compared to respective physical mixtures of cisplatin with axial ligands in test cell lines. Among all three Pt(IV) conjugates, highest dose reduction potential was noted for CP-CBL. In the tested cell lines, CP-CBL treatment was able to attain 6–12 folds cisplatin and 4–10 folds CBL dose reduction in comparison with cisplatin and CBL individual monotherapy, and CP-CBL treatment resulted in 2–3 folds cisplatin and 2–4 folds CBL dose reduction when compared with cisplatin and CBL combination therapy. Notable dose reduction potential of CP-CBL may further help in reducing highly dose-dependent systemic toxicities of cisplatin such as nephrotoxicity.

Overall, all synthesized Pt(IV) conjugates exhibited significantly improved broad-spectrum antiproliferative activity, enhanced therapeutic synergy, and remarkable potential to attain equivalent activity at a significantly reduced cisplatin dose which could help to minimize systemic toxicities. The results also highlighted that Pt(IV) prodrug formation is a more effective strategy to attain enhanced activity, gain better therapeutic synergy, and achieve higher cisplatin dose reduction than combination therapy of cisplatin with axial ligands.

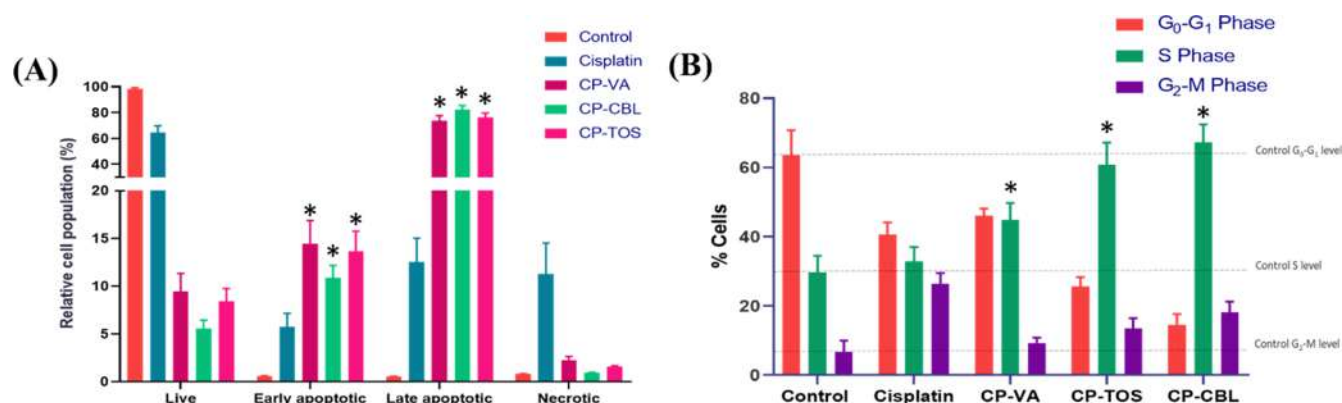


**Figure 5.** Flow cytometric analysis in MDA-MB-231 cells. (A) apoptosis status; (B) cell cycle pattern after treatment with different test samples, that is, free cisplatin, CP-VA, CP-TOS, and CP-CBL. Herein, the concentration of each test compound was 5  $\mu$ M; statistical significance (\* $p$  < 0.001) compared with cisplatin by two-way ANOVA.

**4.2.4. Cellular Drug Uptake.** Extent of cellular drug uptake is the key determinant for therapeutic effectiveness in chemotherapy. Drugs with optimum lipophilicity show higher cellular internalization than most hydrophilic or charged molecules. Cisplatin being a poorly lipophilic molecule shows limited cellular drug internalization. Additionally, cellular internalization of cisplatin is critically dependent on active transport through organic cation transporters (OCT1, OCT2, OCT3) and copper transporters (Ctr1 and Ctr2).<sup>38</sup> Therefore, the slightest alteration in transporter level expression can play a key role in determining the effectiveness of cisplatin therapy. Downregulation of Ctr1 transporters leads to limited cisplatin influx inside cancer cells, and it is widely observed in advanced cancer stages leading to treatment failure.<sup>39</sup>

Development of Pt(IV) agents can assist in enhancing cellular drug uptake by improving drug lipophilicity.<sup>35</sup> In Figure 4A, all synthesized cisplatin Pt(IV) derivatives showed remarkably improved total Pt uptake compared to cisplatin and physical mixture of cisplatin with axial ligands, indicating the critical role of Pt(IV) prodrug formation in modulating drug internalization by altering lipophilicity. Notably, Pt(IV) derivatives with more lipophilic axial ligands (such as CP-TOS and CP-CBL) resulted in relatively higher extent of cellular Pt uptake compared to Pt(IV) agents with low lipophilicity bearing axial ligands (such as CP-VA), showing strong correlation between conjugate's lipophilicity and its cellular uptake. CP-VA-, CP-CBL-, and CP-TOS-treated groups displayed 5.1-, 7.1-, and 9.9-folds increment in the total Pt uptake compared to the cisplatin-treated group. Statistically insignificant difference was noted for Pt uptake levels between cisplatin- and physical mixture-treated groups, proving the exclusive role of axial ligand conjugation in improving the cellular uptake of Pt(IV) derivatives. Ctr1 transporters are considered as a critical regulator for cisplatin cellular influx. Therefore, Pt uptake in the presence of competitive Ctr1 inhibitor (copper sulfate - 1 mM) was tested to analyze the influence of Ctr1 transporters in the uptake of designed Pt(IV) agents. In the presence of Ctr1 inhibitor, cisplatin- and physical mixture (cisplatin + axial ligand)-treated cells showed significant reduction (~2–3 fold) in Pt uptake, indicating strong dependency on Ctr1 in the cisplatin uptake process. On the contrary, CP-VA, CP-CBL, and CP-TOS showed relatively lower reduction in cellular Pt uptake even in the presence of Ctr1 inhibitor. Despite Ctr1 inhibition, the cellular Pt uptake in the Pt(IV) conjugate-treated groups was

appreciably higher than cisplatin- and physical mixture-treated groups. After Ctr1 inhibition, the difference in cellular Pt uptake between cisplatin and Pt(IV) derivatives was significantly higher (CP-VA, CP-TOS, and CP-CBL—10.6-, 26.8- and 17.6-folds, respectively).

These observations proved that the cellular uptake process for cisplatin Pt(IV) conjugates have reduced Ctr1 dependency, and it could help in minimizing the risk of chemoresistance development through Ctr1 downregulation. Moreover, the designed Pt(IV) conjugates may prove to be effective in treating advanced cancer stages where cisplatin therapy is ineffective due to Ctr1 downregulation.

**4.2.5. GSH Assay.** Cellular GSH acts as a cisplatin sequestering agent and reduces the effective cisplatin concentration available for DNA damage. Elevation in cellular GSH levels is closely associated with cisplatin resistance development and therapeutic failure for cisplatin treatment in advanced cancers.<sup>38</sup> Normally, cisplatin gets deactivated through its binding to GSH, and GSH-cisplatin complex is effluxed out of cells. On the contrary, for cisplatin Pt(IV) prodrugs, cellular GSH is necessary to convert prodrugs into active form, that is, cisplatin. GSH acts as a one-electron reducing agent and converts Pt(IV) prodrug into cisplatin and axial ligands through electron transfer reaction. Thus, the synthesized cisplatin Pt(IV) derivatives could favorably utilize elevated cellular GSH levels in resistant cancer cells to get converted into cisplatin by cleaving axial ligands. Utilization of cellular GSH for prodrug conversion results in cellular GSH depletion which could further help in minimizing the deactivation of cisplatin released from the Pt(IV) prodrug.<sup>40</sup> In Figure 4B, the GSH depleting effect of cisplatin Pt(IV) conjugates was distinctly observed compared to cisplatin. Therefore, the developed Pt(IV) conjugates may prove to be effective in treating resistant cancers where elevated GSH levels lead to ineffective cisplatin therapy, and the GSH depleting effect of these conjugates could further help reduce intracellular cisplatin detoxification.

**4.2.6. ROS Production.** Cisplatin treatment is reported to increase cellular ROS levels which assist in triggering apoptosis cascade.<sup>41</sup> Therefore, the cellular ROS level was determined after treating the cells with cisplatin and cisplatin Pt(IV) conjugates. From the green fluorescent intensity, it was observed that treatment with Pt(IV) conjugates resulted in higher ROS generation compared to cisplatin. Higher ROS levels in the Pt(IV) conjugate-treated groups could be the



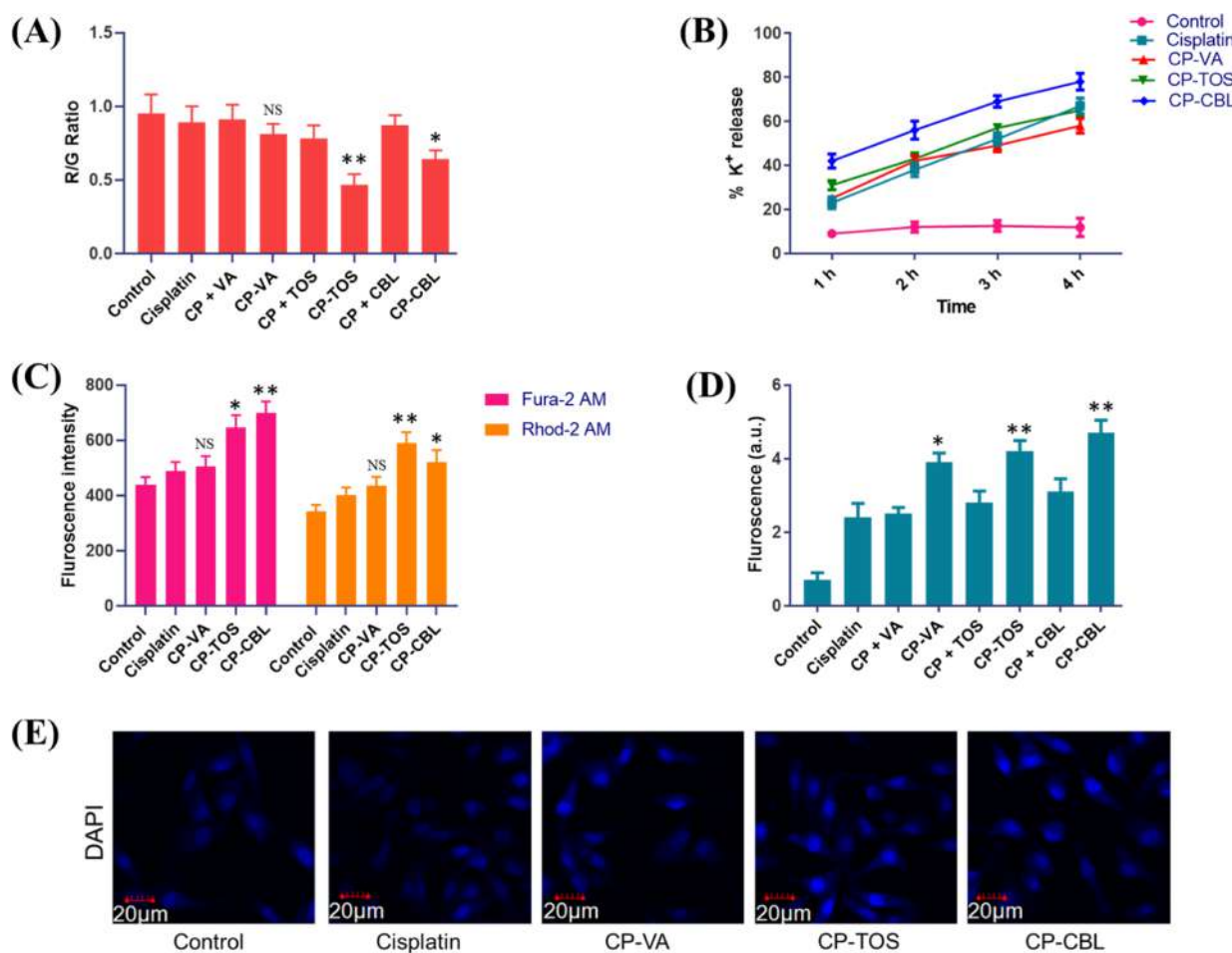


**Figure 6.** (A) Mitochondrial membrane potential analysis by JC1 assay in MDA-MB-231 cells after treatment with test groups, where R denotes the red fluorescence of mitochondrial J aggregates and G denotes the green fluorescence of cytosolic J monomers; statistical significance ( $*p < 0.01$ ,  $**p < 0.0001$ , NS—statistically insignificant) compared with control by one-way ANOVA. (B) Percent of extracellular K<sup>+</sup> ions released from MDA-MB-231 cells after 1, 2, 3, and 4 h incubation with test groups. (C) Analysis of cytosolic and mitochondrial Ca<sup>2+</sup> levels in MDA-MB-231 cells after drug treatment through Fura-2 AM and Rhod-2AM using a spectrofluorometer; statistical significance ( $*p < 0.001$ ,  $**p < 0.0001$ ) compared with cisplatin by two-way ANOVA. (D) Caspase-3 levels in MDA-MB-231 cells after treatment with cisplatin, cisplatin + axial ligand physical mixtures, and cisplatin(IV) conjugates; statistical significance ( $*p < 0.001$ ,  $**p < 0.0001$ ) compared with cisplatin by one-way ANOVA. (E) Hoechst staining of MDA-MB-231 cells after treatment with test compounds. Initiation of nuclear condensation represented by bright white region in the center of cells.

result of relatively higher extent of drug internalization for conjugates. Out of all three Pt(IV) conjugates, CP-CBL showcased the highest ROS level which could possibly help to trigger apoptosis induction (Figure 4C).

**4.2.7. Apoptosis Assay.** Apoptosis assay was carried out in MDA-MB-231 cells to test the effectiveness of CP-VA, CP-TOS, and CP-CBL conjugates to induce cellular apoptosis. After drug treatment, all three Pt(IV) conjugates displayed a significant shift in cell population to early and late apoptotic phases compared to cisplatin (Figure 5A). Overall, the results aligned with antiproliferative activity data and combinedly consolidated the improved apoptosis-inducing potential of dual-action CP conjugates. Synergistic multitargeted activity imparted by cisplatin with axial ligands and improved cellular Pt internalization could be the possible reason for improved apoptosis induction.

**4.2.8. Cell Cycle Analysis.** Cell cycle arrest pattern manifested by cisplatin and cisplatin Pt(IV) conjugates could be substantially distinct from each other due to the presence of axial ligand in the structure of Pt(IV) analogues. Axial ligands get cleaved from Pt(IV) prodrugs in the intracellular reducing

environment and show their individual therapeutic activity along with the parent drug, cisplatin. Therefore, depending on the selection of axial ligand and its pharmacological activity, the cell cycle arrest pattern for cisplatin and its Pt(IV) prodrug may diverge from each other. Alteration in the cell cycle arrest phases for CP-VA, CP-TOS, and CP-CBL compared to cisplatin was clearly observed. As shown in Figure 5B, a significant reduction in cell population in the G<sub>0</sub>–G<sub>1</sub> phase and the subsequent rise in cell population at the S phase was observed in all three Pt(IV) conjugates compared to no treatment control. In the S phase of the cell cycle, the cellular DNA content gets doubled; therefore, G<sub>1</sub>/S checkpoint is highly critical to inhibit cell proliferation by controlling cellular signals associated with transportation and integration of molecules into the nucleus. In the cell cycle analysis after treatment with Pt(IV) conjugates, the cell population in the S phase and G<sub>0</sub>–G<sub>1</sub> phase was found to be increased and decreased, respectively. This pattern of cell cycle arrest could indicate increased DNA damaging ability and enhanced antiproliferative potential of developed Pt(IV) conjugates.<sup>42,43</sup> In CP-VA, axial ligand VA acts as the HDAC inhibitor,

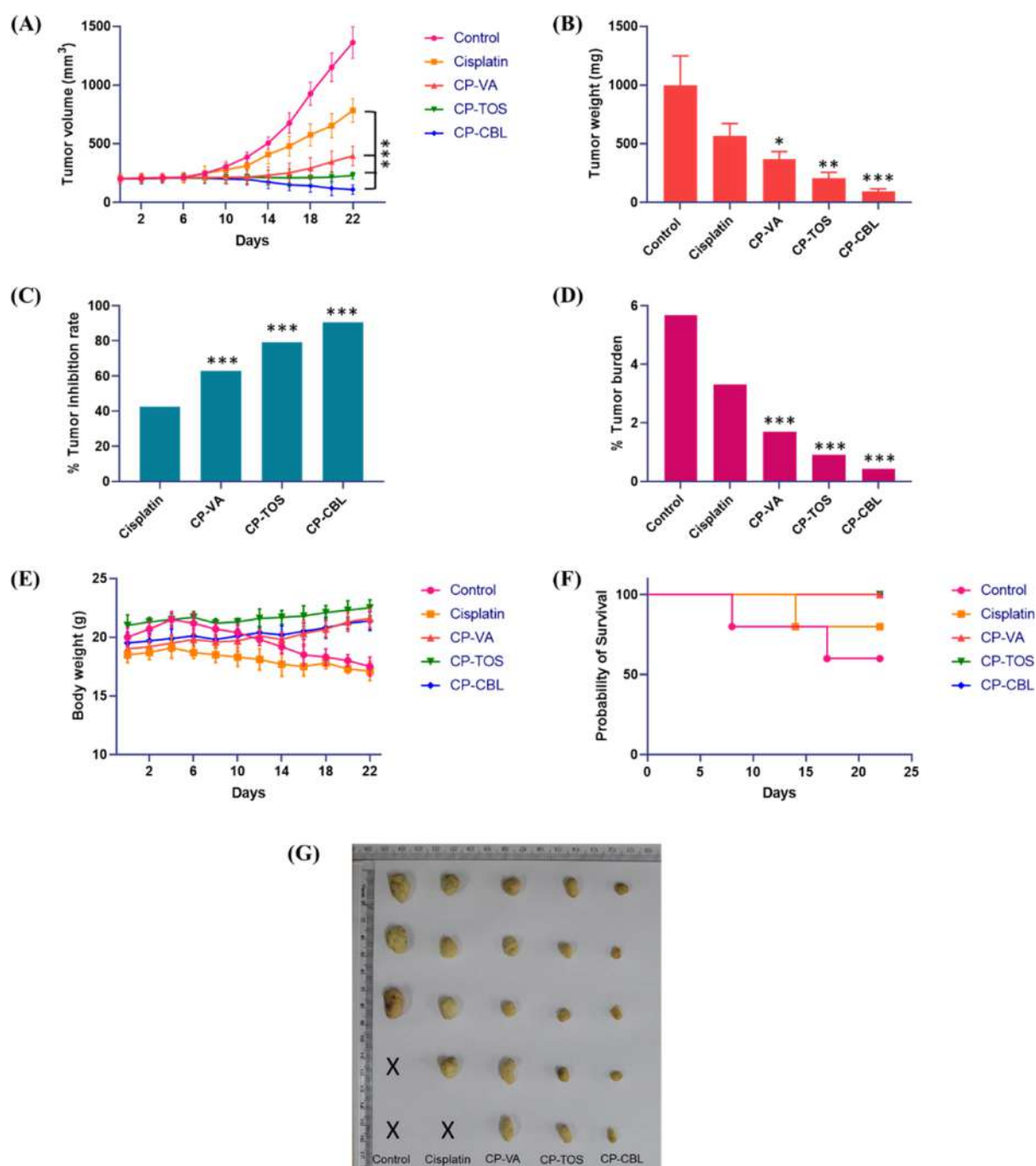


**Figure 7.** In vivo anticancer efficacy of cisplatin and designed cisplatin(IV) derivatives, (A) Tumor volume change over the study duration. (B) Tumor weight in each test group after completion of study. (C) Percent tumor inhibition rate for each test group. (D) Percent tumor burden for each test group at the end of study. (E) Change in body weight for each test group over the study duration. (F) Survival rate for each test group at the end of study. (G) Images of tumors excised from animals after completion of treatment with test groups (X—represent animal death before completion of study duration); statistical significance (\* $p < 0.05$ , \*\* $p < 0.001$ , \*\*\* $p < 0.0001$ ) compared with cisplatin by one-way/two-way ANOVA, wherever applicable.

increasing the accessibility of DNA toward attack by cisplatin, while in the case of CP-CBL, CBL is the DNA alkylator, which could result in dual DNA damage through cisplatin and CBL. The highest extent of S phase arrest observed for the CP-CBL group was indicative of the dual DNA damaging potential of CP-CBL.

**4.2.9. Mitochondrial Membrane Potential Analysis.** Mitochondrial cell death pathways play a pivotal role in the apoptosis process. Mitochondrial membrane potential is one of

the important biological indicators of mitochondrial functioning. It controls critical cellular activities such as ATP production, maintenance of cellular pH, redox balance, cell proliferation rate, and cell death cycle. Alteration of mitochondrial membrane potential is a hallmark for mitochondrial impairment and has been closely linked to the cellular apoptosis process. In a study, mitochondrial depolarization was evaluated by the JC1 assay. JC1 is the mitochondrial membrane potential sensitive dye, and it

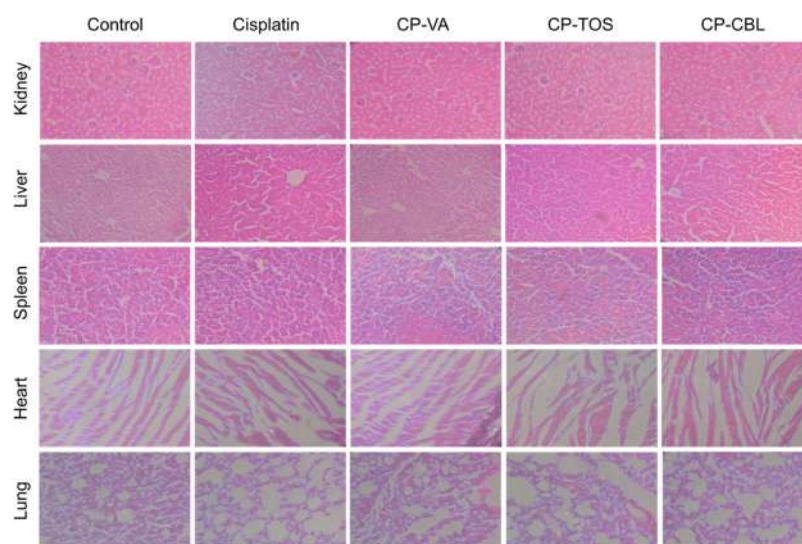


**Figure 8.** In vivo toxicity analysis of cisplatin and designed cisplatin(IV) derivatives in healthy Swiss albino mice. Estimation of vital organ toxicity through organ histopathology analysis using H&E-stained images of kidney, liver, spleen, heart, and lung samples harvested from animals treated with test compounds.

shows a shift of fluorescence from red (mitochondria) to green (cytosol) on collapse of the mitochondrial membrane potential. Therefore, mitochondrial depolarization can be estimated from the red/green (R/G) fluorescence intensity ratio. In Figure 6A, all three cisplatin conjugates resulted in mitochondrial membrane depolarization at higher intensity than cisplatin and their corresponding physical mixtures. Out of all groups, the highest mitochondrial membrane depolarization was noted in the CP-TOS-treated group, suggestive of mitochondrial action presented by TOS.

**4.2.10. Studying Disruption of Cellular Ion Homeostasis.** Apoptotic events are marked by cellular features such as in cellular  $K^+$  leakage and cellular  $Ca^{2+}$  level imbalance.<sup>44</sup> Therefore, level of these ions after drug treatment was monitored. After 5  $\mu M$  drug treatment, cell suspension samples were tested for the presence of  $K^+$  ions. Time-dependent increase in  $K^+$  ions was observed in all drug-treated groups. CP-CBL-treated cells showcased highest  $K^+$  ion leakage<sup>45</sup> (Figure 6B). Calcium ions play a critical role in apoptosis induction, and mitochondrial  $Ca^{2+}$  uptake is closely associated with the activation of apoptotic factors such as caspases and cytochrome *c*. Therefore, analysis of  $Ca^{2+}$  level in cytosol and mitochondria was studied as an indicator for initiation of apoptotic events using cytosolic  $Ca^{2+}$ -specific reagent, Fura-2AM, and mitochondrial  $Ca^{2+}$ -specific reagent, Rhod-2AM (Figure 6C). Cisplatin conjugates CP-VA, CP-TOS, and CP-CBL exhibited increased mitochondrial  $Ca^{2+}$  uptake as well as cytosolic  $Ca^{2+}$  levels. The highest mitochondrial  $Ca^{2+}$  uptake was observed in the CP-TOS group, which is well supported by the mitochondrial action of TOS.<sup>44</sup>

**4.2.11. Nuclear Staining.** Cisplatin primarily acts through DNA cross-linking and further induces apoptosis cascade. Nuclear chromatin condensation, genomic DNA fragmentation, and cell membrane blebbing, are hallmark features for terminal apoptosis stages. During apoptosis, the chromatin structure changes from a heterogeneous, genetically active network to an inert and highly condensed structure. After staining with DNA-binding nuclear dyes, such as Hoechst 33342, the compacted nuclear chromatin gets stained brighter

than the active chromatin from nonapoptotic cells, and the condensed nuclei can be easily identified by fluorescence microscopy (qualitative detection). The intensity of fluorescence after nuclear condensation can also be used to estimate the DNA damaging intensity of test compounds roughly. In Figure 6E, all three Pt(IV) conjugates exhibited a higher level of nuclear condensation than cisplatin, which could be observed from the fluorescent intensity of bright spots in cells. Higher cellular drug uptake and enhanced DNA damaging ability of Pt(IV) conjugates due to dual-drug action could be the reason for this observation.<sup>46</sup>

**4.2.12. Caspase-3 Assay.** Caspase-3 is one of the important apoptosis executioners and considered as a key enzyme in facilitating apoptosis. Caspase-3 activation and triggering of further apoptosis cascade is one of the important molecular features of cisplatin-induced apoptosis.<sup>47</sup> After drug treatment, protein aliquots for each test group were separated and exposed to caspase-3 substrate (*N*-Acetyl-Asp-Glu-Val-Asp-7-amido-4-methylcoumarin) to determine the caspase-3 levels induced after drug treatment. All three cisplatin conjugates resulted in higher caspase-3 level expression compared to cisplatin and their corresponding physical mixtures, denoting improved apoptosis induction potential for Pt(IV) derivatives (Figure 6D). Higher cellular drug uptake and synergistic anticancer activity of cisplatin and axial ligands could be the possible reasons for this observation.

**4.3. In Vivo Studies.** **4.3.1. Anticancer Efficacy Study.** The anticancer efficacy of designed Pt(IV) conjugates was tested in 4T1 cell line-induced TNBC model in BALB/c mice. At the end of the study, all three conjugate-treated groups displayed significant tumor volume and tumor weight reduction compared to the cisplatin-treated group. CP-VA, CP-TOS, and CP-CBL treatment resulted in 1.9-, 3.4-, and 7.2-folds higher tumor volume reduction and 1.5-, 2.8-, and 6.1-folds higher tumor weight reduction than cisplatin therapy (Figure 7A,B). The therapeutic effectiveness of Pt(IV) derivatives over cisplatin therapy was reflected in the percent tumor inhibition rate and the percent tumor burden (Figure 7C,D). Out of the three conjugates, CP-CBL showcased the highest reduction in tumor burden and tumor inhibition rate,



indicative of potent anticancer activity due to dual-DNA damaging action. Body weight reduction was prominent in control and cisplatin-treated animals, while Pt(IV) derivative-treated groups showed insignificant body weight loss, indicating reduced toxicity risk (Figure 7E). Treatment with Pt(IV) conjugates resulted in better survival results with no observed animal mortality than cisplatin and control groups (Figure 7F).

**4.3.2. Toxicity Analysis.** Cisplatin treatment is marked with distinct dose-dependent nephrotoxicity.<sup>48</sup> Cisplatin(IV) pro-drug formation may assist in reducing systemic toxicities by reducing the kinetic interaction of cisplatin with blood components and altering drug biodistribution by virtue of improved lipophilicity.<sup>15</sup> Also, therapeutic synergism of cisplatin with axial ligands, remarkable DRI values, and enhanced cellular uptake for Pt(IV) derivatives could result in significant cisplatin dose reduction to limit systemic toxicities. The risk of systemic toxicities from CP-VA, CP-TOS, and CP-CBL treatment was estimated from blood biomarker levels such as AST, ALT, and ALP (indicative of hepatotoxicity) and BUN and creatinine (indicative of nephrotoxicity). Renal damage biomarker levels (MDA, IL-6, and TNF- $\alpha$ ) were analyzed from the kidney homogenate obtained from drug-treated animals. Levels of all systemic toxicity as well as renal damage biomarkers after Pt(IV) conjugate treatment were found to be significantly lower than cisplatin-treated group proving the better safety profile of cisplatin(IV) conjugates (refer the Supporting Information). Organ histopathology data were also in-line with the trend for biomarker levels and showed no vital organ toxicity. No major signs of nephrotoxicity such as tubular degeneration, necrosis, or glomerular atrophy were observed for Pt(IV) conjugate-treated groups<sup>40</sup> (Figure 8).

## 5. CONCLUSIONS

Synthesised cisplatin(IV) conjugates, that is, CP-VA, CP-TOS, and CP-CBL showcased significant improvement in anticancer activity and substantial cisplatin dose reduction potential along with strong therapeutic synergism between cisplatin and axial ligands. All conjugates displayed remarkable enhancement in cellular drug uptake and reduced dependence on the Ctrl pathway for cellular drug uptake compared to cisplatin. GSH depleting effect by Pt(IV) conjugates and improved drug uptake may play a pivotal role in tackling cisplatin resistance development. Designed cisplatin(IV) conjugates displayed their anticancer activity by attacking multiple cellular targets such as nucleus, mitochondria, and histones, which could enhance therapeutic efficacy by targeting nonoverlapping pathways of cancer progression. In vivo studies highlighted the improved anticancer efficacy and substantially reduced the risk of nephrotoxicity for cisplatin(IV) conjugate treatment. CP-CBL showcased the highest anticancer efficacy in TNBC pertaining to its dual-DNA damaging activity out of the three conjugates. Overall results supported the role of designed conjugates in improving therapeutic efficacy, attaining dose reduction, and ensuring the safety of platinum-based chemotherapy in TNBC management.

## ■ ASSOCIATED CONTENT

### SI Supporting Information

The Supporting Information is available free of charge at <https://pubs.acs.org/doi/10.1021/acsbiomaterials.1c01582>.

<sup>1</sup>H NMR, <sup>13</sup>C NMR, and mass spectrum of CP-VA, CP-TOS, and CP-CBL, stability of designed conjugates, antiproliferative activity in noncancerous cells, cell viability plots in cancerous cells, apoptosis and cell cycle analysis, and in vivo toxicity biomarker levels (PDF)

## ■ AUTHOR INFORMATION

### Corresponding Author

**Sanyog Jain** – Centre for Pharmaceutical Nanotechnology, Department of Pharmaceutics, National Institute of Pharmaceutical Education and Research (NIPER), Mohali 160062 Punjab, India; [orcid.org/0000-0002-0688-9563](https://orcid.org/0000-0002-0688-9563); Email: [sanyogjain@niper.ac.in](mailto:sanyogjain@niper.ac.in), [sanyogjain@rediffmail.com](mailto:sanyogjain@rediffmail.com)

### Authors

**Tushar Date** – Centre for Pharmaceutical Nanotechnology, Department of Pharmaceutics, National Institute of Pharmaceutical Education and Research (NIPER), Mohali 160062 Punjab, India

**Kaushik Kuche** – Centre for Pharmaceutical Nanotechnology, Department of Pharmaceutics, National Institute of Pharmaceutical Education and Research (NIPER), Mohali 160062 Punjab, India

**Dasharath Chaudhari** – Centre for Pharmaceutical Nanotechnology, Department of Pharmaceutics, National Institute of Pharmaceutical Education and Research (NIPER), Mohali 160062 Punjab, India

**Rohan Ghadi** – Centre for Pharmaceutical Nanotechnology, Department of Pharmaceutics, National Institute of Pharmaceutical Education and Research (NIPER), Mohali 160062 Punjab, India

**Deepak Kumar Sahel** – Department of Pharmacy, Birla Institute of Technology and Science-Pilani, Pilani 333031 Rajasthan, India

**Deepak Chitkara** – Department of Pharmacy, Birla Institute of Technology and Science-Pilani, Pilani 333031 Rajasthan, India; [orcid.org/0000-0003-4174-7664](https://orcid.org/0000-0003-4174-7664)

Complete contact information is available at:

<https://pubs.acs.org/doi/10.1021/acsbiomaterials.1c01582>

### Notes

The authors declare no competing financial interest.

## ■ ACKNOWLEDGMENTS

The authors are grateful to the Director, NIPER SAS Nagar, for providing infrastructure for research work. We also appreciate the support of Neon Laboratories Ltd, India, for providing cisplatin research sample.

## ■ REFERENCES

- (1) Dent, R.; Trudeau, M.; Pritchard, K. I.; Hanna, W. M.; Kahn, H. K.; Sawka, C. A.; Lickley, L. A.; Rawlinson, E.; Sun, P.; Narod, S. A. Triple-negative breast cancer: clinical features and patterns of recurrence. *Des. Monomers Polym.* **2007**, *13*, 4429–4434.
- (2) Cleator, S.; Heller, W.; Coombes, R. C. Triple-negative breast cancer: therapeutic options. *Lancet Oncol.* **2007**, *8*, 235–244.
- (3) Bianchini, G.; Balko, J. M.; Mayer, I. A.; Sanders, M. E.; Gianni, L. Triple-negative breast cancer: challenges and opportunities of a heterogeneous disease. *Nat. Rev. Clin. Oncol.* **2016**, *13*, 674.
- (4) Sirohi, B.; Arnedos, M.; Popat, S.; Ashley, S.; Nerurkar, A.; Walsh, G.; Johnston, S.; Smith, I. E. Platinum-based chemotherapy in triple-negative breast cancer. *Ann. Oncol.* **2008**, *19*, 1847–1852.

- (5) Pandey, J. G. P.; Balolong-Garcia, J. C.; Cruz-Ordinario, M. V. B.; Que, F. V. F. Triple negative breast cancer and platinum-based systemic treatment: a meta-analysis and systematic review. *BMC Cancer* **2019**, *19*, 1065.
- (6) Telli, M. Optimizing chemotherapy in triple-negative breast cancer: the role of platinum. *Am. Soc. Clin. Oncol. Educ. Book* **2014**, *34*, e37–e42.
- (7) Guo, J.; Xu, B.; Han, Q.; Zhou, H.; Xia, Y.; Gong, C.; Dai, X.; Li, Z.; Wu, G. Ferroptosis: a novel anti-tumor action for cisplatin. *Cancer Res. Treat.* **2018**, *50*, 445.
- (8) Macciò, A.; Madeddu, C. Cisplatin: an old drug with a newfound efficacy—from mechanisms of action to cytotoxicity. *Expert Opin. Pharmacother.* **2013**, *14*, 1839–1857.
- (9) Florea, A.-M.; Büsselberg, D. Cisplatin as an anti-tumor drug: cellular mechanisms of activity, drug resistance and induced side effects. *Cancers* **2011**, *3*, 1351–1371.
- (10) de Biasi, A. R.; Villena-Vargas, J.; Adusumilli, P. S. Cisplatin-induced antitumor immunomodulation: a review of preclinical and clinical evidence. *Clin. Cancer Res.* **2014**, *20*, 5384–5391.
- (11) Siddik, Z. H. Cisplatin: mode of cytotoxic action and molecular basis of resistance. *Oncogene* **2003**, *22*, 7265–7279.
- (12) Galluzzi, L.; Vitale, I.; Michels, J.; Brenner, C.; Szabadkai, G.; Harel-Bellan, A.; Castedo, M.; Kroemer, G. Systems biology of cisplatin resistance: past, present and future. *Cell Death Dis.* **2014**, *5*, No. e1257.
- (13) Hill, D. P.; Harper, A.; Malcolm, J.; McAndrews, M. S.; Mockus, S. M.; Patterson, S. E.; Reynolds, T.; Baker, E. J.; Bult, C. J.; Chesler, E. J. Cisplatin-resistant triple-negative breast cancer subtypes: multiple mechanisms of resistance. *BMC Cancer* **2019**, *19*, 1039.
- (14) Wexselblatt, E.; Gibson, D. What do we know about the reduction of Pt(IV) pro-drugs? *J. Inorg. Biochem.* **2012**, *117*, 220–229.
- (15) Johnstone, T. C.; Suntharalingam, K.; Lippard, S. J. The Next Generation of Platinum Drugs: Targeted Pt(II) Agents, Nanoparticle Delivery, and Pt(IV) Prodrugs. *J. Inorg. Biochem.* **2016**, *116*, 3436–3486.
- (16) Yang, J.; Sun, X.; Mao, W.; Sui, M.; Tang, J.; Shen, Y. Conjugate of Pt(IV)-Histone Deacetylase Inhibitor as a Prodrug for Cancer Chemotherapy. *Mol. Pharm.* **2012**, *9*, 2793–2800.
- (17) Novohradsky, V.; Zerankova, L.; Stepankova, J.; Vrana, O.; Raveendran, R.; Gibson, D.; Kasparkova, J.; Brabec, V. New insights into the molecular and epigenetic effects of antitumor Pt(IV)-valproic acid conjugates in human ovarian cancer cells. *Biochem. Pharmacol.* **2015**, *95*, 133–144.
- (18) Chen, F.; Xu, G.; Qin, X.; Jin, X.; Gou, S. Hybrid of DNA-targeting Chlorambucil with Pt(IV) Species to Reverse Drug Resistance. *J. Pharmacol. Exp. Ther.* **2017**, *363*, 221–239.
- (19) Garmpis, N.; Damaskos, C.; Garmpi, A.; Kalampokas, E.; Kalampokas, T.; Spartalis, E.; Daskalopoulou, A.; Valsami, S.; Kontos, M.; Nonni, A. Histone deacetylases as new therapeutic targets in triple-negative breast cancer: Progress and promises. *Cancer Genomics Proteomics* **2017**, *14*, 299–313.
- (20) Ossovskaya, V.; Wang, Y.; Budoff, A.; Xu, Q.; Lituev, A.; Potapova, O.; Vansant, G.; Monforte, J.; Daraselia, N. Exploring molecular pathways of triple-negative breast cancer. *Genes Cancer* **2011**, *2*, 870–879.
- (21) Jamdade, V. S.; Sethi, N.; Mundhe, N. A.; Kumar, P.; Lahkar, M.; Sinha, N. Therapeutic targets of triple-negative breast cancer: a review. *Br. J. Pharmacol.* **2015**, *172*, 4228–4237.
- (22) Göttlicher, M.; Minucci, S.; Zhu, P.; Krämer, O. H.; Schimpf, A.; Giavara, S.; Sleeman, J. P.; Coco, F. L.; Nervi, C.; Pelicci, P. G. Valproic acid defines a novel class of HDAC inhibitors inducing differentiation of transformed cells. *EMBO J.* **2001**, *20*, 6969–6978.
- (23) Fuertes, M.; Castilla, J.; Alonso, C.; Pérez, J. Cisplatin biochemical mechanism of action: from cytotoxicity to induction of cell death through interconnections between apoptotic and necrotic pathways. *Curr. Med. Chem.* **2003**, *10*, 257–266.
- (24) Shiao, C.-W.; Huang, J.-W.; Wang, D.-S.; Weng, J.-R.; Yang, C.-C.; Lin, C.-H.; Li, C.; Chen, C.-S.  $\alpha$ -Tocopheryl Succinate Induces Apoptosis in Prostate Cancer Cells in Part through Inhibition of Bcl-xL/Bcl-2 Function. *J. Biol. Chem.* **2006**, *281*, 11819–11825.
- (25) Neuzil, J.; Weber, T.; Gellert, N.; Weber, C. Selective cancer cell killing by  $\alpha$ -tocopheryl succinate. *Br. J. Cancer* **2001**, *84*, 87–89.
- (26) Yu, W.; Sanders, B. G.; Kline, K. RRR- $\alpha$ -tocopheryl succinate-induced apoptosis of human breast cancer cells involves Bax translocation to mitochondria. *Cancer Res.* **2003**, *63*, 2483–2491.
- (27) Di Antonio, M.; McLuckie, K. I. E.; Balasubramanian, S. Reprogramming the mechanism of action of chlorambucil by coupling to a G-quadruplex ligand. *J. Am. Chem. Soc.* **2014**, *136*, 5860–5863.
- (28) Ciaccio, P. J.; Tew, K. D.; LaCreta, F. P. Enzymatic conjugation of chlorambucil with glutathione by human glutathione S-transferases and inhibition by ethacrynic acid. *Biochem. Pharmacol.* **1991**, *42*, 1504–1507.
- (29) Hall, M. D.; Dillon, C. T.; Zhang, M.; Beale, P.; Cai, Z.; Lai, B.; Stampfl, A. P. J.; Hambley, T. W. The cellular distribution and oxidation state of platinum(II) and platinum(IV) antitumor complexes in cancer cells. *JBIC, J. Biol. Inorg. Chem.* **2003**, *8*, 726–732.
- (30) Bartoli, G.; Bosco, M.; Carlone, A.; Dalpozzo, R.; Marcantoni, E.; Melchiorre, P.; Sambri, L. Reaction of dicarbonates with carboxylic acids catalyzed by weak Lewis acids: general method for the synthesis of anhydrides and esters. *Synthesis* **2007**, *2007*, 3489–3496.
- (31) Vichai, V.; Kirtikara, K. Sulforhodamine B colorimetric assay for cytotoxicity screening. *Nat. Protoc.* **2006**, *1*, 1112–1116.
- (32) Orellana, E. A.; Kasinski, A. L. Sulforhodamine B (SRB) assay in cell culture to investigate cell proliferation. *Bio-Protoc.* **2016**, *6*, No. e1984.
- (33) Chou, T.-C. Drug combination studies and their synergy quantification using the Chou-Talalay method. *Cancer Res.* **2010**, *70*, 440–446.
- (34) Kyakulaga, A. H.; Aqil, F.; Munagala, R.; Gupta, R. C. Synergistic combinations of paclitaxel and withaferin A against human non-small cell lung cancer cells. *Oncotarget* **2020**, *11*, 1399.
- (35) Ghezzi, A.; Aceto, M.; Cassino, C.; Gabano, E.; Osella, D. Uptake of antitumor platinum(II)-complexes by cancer cells, assayed by inductively coupled plasma mass spectrometry (ICP-MS). *J. Inorg. Biochem.* **2004**, *98*, 73–78.
- (36) Silver, D. P.; Richardson, A. L.; Eklund, A. C.; Wang, Z. C.; Szallasi, Z.; Li, Q.; Juul, N.; Leong, C.-O.; Calogrias, D.; Buraimoh, A.; Fatima, A.; Gelman, R. S.; Ryan, P. D.; Tung, N. M.; De Nicolo, A.; Ganesan, S.; Miron, A.; Colin, C.; Sgroi, D. C.; Ellisen, L. W.; Winer, E. P.; Garber, J. E. Efficacy of neoadjuvant Cisplatin in triple-negative breast cancer. *J. Clin. Oncol.* **2010**, *28*, 1145.
- (37) Poggio, F.; Bruzzzone, M.; Ceppi, M.; Pondé, N. F.; La Valle, G.; Del Mastro, L.; De Azambuja, E.; Lambertini, M. Platinum-based neoadjuvant chemotherapy in triple-negative breast cancer: a systematic review and meta-analysis. *Ann. Oncol.* **2018**, *29*, 1497–1508.
- (38) Makovec, T. Cisplatin and beyond: molecular mechanisms of action and drug resistance development in cancer chemotherapy. *Radiol. Oncol.* **2019**, *53*, 148.
- (39) Kalayda, G. V.; Wagner, C. H.; Jaehde, U. Relevance of copper transporter 1 for cisplatin resistance in human ovarian carcinoma cells. *J. Inorg. Biochem.* **2012**, *116*, 1–10.
- (40) Ling, X.; Tu, J.; Wang, J.; Shajii, A.; Kong, N.; Feng, C.; Zhang, Y.; Yu, M.; Xie, T.; Bharwani, Z.; Aljaeid, B. M.; Shi, B.; Tao, W.; Farokhzad, O. C. Glutathione-responsive prodrug nanoparticles for effective drug delivery and cancer therapy. *ACS Nano* **2018**, *13*, 357–370.
- (41) Marullo, R.; Werner, E.; Degtyareva, N.; Moore, B.; Altavilla, G.; Ramalingam, S. S.; Doetsch, P. W. Cisplatin induces a mitochondrial-ROS response that contributes to cytotoxicity depending on mitochondrial redox status and bioenergetic functions. *PLoS One* **2013**, *8*, No. e81162.
- (42) Zhu, Q.; Hu, J.; Meng, H.; Shen, Y.; Zhou, J.; Zhu, Z. S-Phase cell cycle arrest, apoptosis, and molecular mechanisms of ap1ras homolog member I-induced human ovarian cancer SKOV3 cell lines. *Int. J. Gynecol. Cancer* **2014**, *24*, 629–634.

(43) Skotheim, J. M.; Di Talia, S.; Siggia, E. D.; Cross, F. R. Positive feedback of G1 cyclins ensures coherent cell cycle entry. *Nature* **2008**, *454*, 291–296.

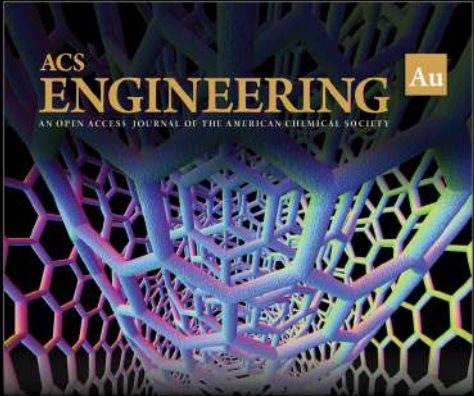
(44) Orrenius, S.; Zhivotovsky, B.; Nicotera, P. Regulation of cell death: the calcium-apoptosis link. *Nat. Rev. Mol. Cell Biol.* **2003**, *4*, 552–565.

(45) Yu, S. P. Regulation and critical role of potassium homeostasis in apoptosis. *Prog. Neurobiol.* **2003**, *70*, 363–386.

(46) Muhammad, N.; Tan, C.-P.; Nawaz, U.; Wang, J.; Wang, F.-X.; Nasreen, S.; Ji, L.-N.; Mao, Z.-W. Multi-action Platinum(IV) Prodrug Containing Thymidylate Synthase Inhibitor and Metabolic Modifier against Triple-Negative Breast Cancer. *Inorg. Chem.* **2020**, *59*, 12632–12642.


(47) Blanc, C.; Deveraux, Q. L.; Krajewski, S.; Jänicke, R. U.; Porter, A. G.; Reed, J. C.; Jaggi, R.; Marti, A. Caspase-3 is essential for procaspase-9 processing and cisplatin-induced apoptosis of MCF-7 breast cancer cells. *Cancer Res.* **2000**, *60*, 4386–4390.


(48) Manohar, S.; Leung, N. Cisplatin nephrotoxicity: a review of the literature. *J. Nephrol.* **2018**, *31*, 15–25.




ACS  
**ENGINEERING** Au  
AN OPEN ACCESS JOURNAL OF THE AMERICAN CHEMICAL SOCIETY

Editor-in-Chief: **Prof. Shelley D. Minteer**, University of Utah, USA

 Deputy Editor:  
**Prof. Vivek Ranade**  
University of Limerick, Ireland

**Open for Submissions** 

pubs.acs.org/engineeringau  ACS Publications  
Most Trusted. Most Cited. Most Read.





# pH sensitive liposomes assisted specific and improved breast cancer therapy using co-delivery of SIRT1 shRNA and Docetaxel

Rajan Swami<sup>a</sup>, Yogesh Kumar<sup>a</sup>, Dasharath Chaudhari<sup>a</sup>, Sameer S. Katiyar<sup>a</sup>, Kaushik Kuche<sup>a</sup>, Parmeshwar B. Katare<sup>b</sup>, Sanjay K. Banerjee<sup>b,c</sup>, Sanyog Jain<sup>a,\*</sup>

<sup>a</sup> Centre for Pharmaceutical Nanotechnology, Department of Pharmaceutics, National Institute of Pharmaceutical Education and Research (NIPER), Sector 67, S.A.S. Nagar (Mohali), Punjab, India

<sup>b</sup> Drug Discovery Research Centre, Translational Health Science and Technology Institute, Faridabad 121001, India

<sup>c</sup> Department of Biotechnology, National Institute of Pharmaceutical Education and Research (NIPER), Guwahati 781101, Assam, India

## ARTICLE INFO

### Keywords:

shRNA  
Docetaxel  
Co-delivery  
pH sensitive liposomes  
Breast cancer

## ABSTRACT

Combining the bio-therapeutics with chemotherapeutic drugs can assist in augmenting the therapeutic standards by increasing the efficacy and decreasing the toxicity. Hence, in the present investigation Docetaxel (DTX) loaded pH-sensitive SIRT1 shRNA complexed lipoplex (DTX-lipoplex) were developed and explored for their improved breast cancer potential. The DTX-lipoplex were prepared by solvent evaporation and rehydration method and were evaluated for various quality attributes (particle size, % entrapment efficiency, hemotoxicity, DNA stability efficiency etc.), *in vitro* drug release, cell culture assays, antitumor efficacy and *in vivo* toxicity. The DTX-lipoplex exhibited a size of ~200 nm and zeta-potential of ~20 mV with ~70% encapsulation. Through systematic *in vitro* and *in vivo* examinations, DTX-lipoplex showed ~3 fold higher DTX titre within the tumor cells thereby significantly reducing the tumor burden (~78%) when compared to the marketed non pH sensitive lipid transfection agent and clinical counterpart i.e. Taxotere®. Thus, to conclude it can be said that co-delivering DTX and SIRT1 shRNA in a single tumor-specific nano-platform can improve the therapeutic potential of current therapy.

## 1. Introduction

Recently, in the field of cancer therapeutics a paradigm shift in the exploration of new, novel and efficacious therapy has been observed [1]. It is predicted that in the imminent future, clinical breakthrough is only possible using integrative approach with recognised disciplines such as chemotherapy, radiotherapy, immunotherapy and gene therapy [2–4]. The prime objective of these therapies is not just limited towards killing cancer cells but is also focused on improving progression free survival of patients with enhanced survival rate and quality of life [5–8].

However, rational selection of therapeutics or bio-therapeutics for achieving synergetic effect is always crucial in designing such future therapies. In case of bio-therapeutics, literature cites that shRNA exhibits lesser off-target effects with multiple target silencing capability and superior efficiency when compared to other nucleic acid based therapeutics [9,10]. These advantages of shRNA, make them a better therapeutic candidate than siRNA and certainly a better contender for

future investigations. Further, a compelling delivery system may enhance the response and can also assist in development of next generation cancer therapeutics. That's where nanotechnology comes into existence.

Among different nanoplatforms, lipidic systems emerged to have an edge over the other systems in terms of better transfection, biocompatibility and ability to deliver multiple therapeutics simultaneously [11,12]. Saad et al. formulated doxorubicin loaded cationic liposomes complexed with siRNA for treating multidrug-resistant lung cancer cells (*in vitro* cell line studies) which revealed enhanced apoptosis index than each of the therapeutic when used individually [13]. Similar results were manifested by Shim et al. wherein Trilysinoyl oleylamide-based cationic liposomes were prepared for systemic co-delivery of siRNA and an anticancer drug [14]. Further, Kim et al. also attempted a combinational therapy using EGFR VIII siRNA and erlotinib in glioblastoma cells and documented promising results in terms of anticancer efficacy in comparison to its naive counterparts [15]. Majority of gene

\* Corresponding author at: Centre for Pharmaceutical Nanotechnology, Department of Pharmaceutics, National Institute of Pharmaceutical Education and Research, Sector 67, S.A.S. Nagar (Mohali), Punjab 160062, India.

E-mail address: [sanyogjain@niper.ac.in](mailto:sanyogjain@niper.ac.in) (S. Jain).

<https://doi.org/10.1016/j.msec.2020.111664>

Received 21 June 2020; Received in revised form 25 September 2020; Accepted 20 October 2020

Available online 22 October 2020

0928-4931/© 2020 Elsevier B.V. All rights reserved.

delivery based reports rests upon improving the issues pertaining to their low transfection efficiency, systemic stability and lack of endosomal escape. However, inefficient uptake, nonspecific distribution leading to undesired toxicity and sub-therapeutic effects are still some of the unresolved issues which needs to be addressed for achieving improved therapy [16]. With reference to that, researchers have tried employing either novel lipids or active ligands for improving the tumor cell specific delivery [8,17–22]. But most of the available reports failed to focus on the toxicity aspect of the system which actually affects the fate of the patient responsiveness towards advanced therapies. Moreover, even after active targeting, the effective release of cargo from endosome still remains to be a challenge [6]. Hence, use of pH sensitive liposomal platform in the development, is a decisive step in the direction of gene/drug co-delivery [23–25]. Additionally, all published reports have employed siRNA (not shRNA) as bio-therapeutic molecule and hence may lack advanced approach.

In humans, numerous forms of cancer including colon, brain, lymphoma and breast, have shown considerably augmented expression of sirtuin 1 (SIRT1) [26]. This role of SIRT1 is multifaceted. SIRT1 over-expression in cancer cells decreases the cargo penetration owing to the stimulation and expression of efflux transporters along with multidrug resistance receptors. This enables cells to exhibit hyper-proliferation, anti-apoptotic rewards and encourages DNA damage repair. Such manifestation can also lead to exhibit genetic mutations under therapeutic stress and can transform the tumor microenvironment into a drug resistant environment [27,28]. This leads to a condition where the drug titre within the tumor cells will be reduced significantly. Hence, with this present investigation, SIRT1 silencing RNA (SIRT1 shRNA) molecule is employed along with a model drug *i.e.* Docetaxel (DTX) for elevating the therapy standards.

DTX, a microtubule hyper stabilizing agent has been considered as the potent drug to treat breast cancer. DTX is commercially marketed as Taxotere® or Docefrez®. Taxotere® contains dehydrated alcohol (0.395 mg/mL) and high surfactant concentration for achieving the desired solubility of DTX, which leads to multiple *in vivo* toxic reactions [29,30]. Moreover, efflux transporters reduce the drug titre within the cell leading to decreased therapeutic efficacy of DTX [31]. The SIRT1 shRNA can inhibit the production of SIRT1 and can thus sensitize the drug resistant cells by barring the expression of efflux transporter and thereby increasing the cytoplasmic DTX titre (further investigation is demanded). Therefore, it can unlock a window of time in which the resistant cells will transiently become sensitized to co-delivered anti-cancer drug. Thereby overcoming the drug resistance with combinational innate cytotoxic effect of the co-delivered shRNA.

Regardless of the significant role of SIRT1 in cancer cell regulation, it has not been adequately examined as a novel therapeutic target for shRNA, either as a single or integrated therapy. To the best of our knowledge, no reports have ever been presented for such myriad combinations (SIRT1 shRNA, Docetaxel, pH sensitive cationic liposomes) to increase the efficacy and to reduce the toxicity of the formulation. The proposed hypothesis was proved by series of *in vitro* and *in vivo* investigations.

## 2. Material and methods

DTX was provided as the kind gift by Therdose Pharma, Hyderabad, India. 1, 2-dioleoylsn-glycero-3-phosphoethanolamine (DOPE), 1,2-Dioleoyloxy-3-trimethylammoniumpropanchloride (DOTAP) and phosphatidylcholine (PC) were acquired as a generous gift sample from Lipoid, Germany. Mannitol, Coumarin-6, Triton X-100, 7,12-Dimethylbenz[a]anthracene (DMBA) were procured from Sigma Aldrich, USA. Lipofectamine™2000 was purchased from Invitrogen life technologies, USA. Cholesterol, Ethidium bromide (EtBr), DNA endonucleases enzyme and agarose were purchased from HiMedia®, Mumbai, India. DNA standard ladder was procured from BioPrep. DNA gel loading dye from Thermo Fisher Scientific, USA. Blood urea nitrogen (BUN), alanine transaminase

(ALT), creatinine and aspartate transaminase (AST) kits were procured from Accurex Biomedical Pvt. Ltd., Mumbai, India. SIRT1 shRNA (8.7 kb) encoded for green fluorescence protein (GFP) was procured from Dharmacon (Colorado, USA). Cell repository facility of National Centre for Cell Sciences (NCCS) Pune, India provided MCF-7 (Human breast carcinoma), MDA-MB-231 (Breast Adenocarcinoma) cell lines. All other chemicals and reagents were of analytical grade and procured from local suppliers.

### 2.1. Preparation and optimization of liposomes

For the preparation of liposomes, thin film hydration method was employed [32]. Briefly, different lipids (DOTAP, DOPE, Cholesterol, PC) with different molar ratios were dissolved in organic solvent mixture (chloroform: methanol:: 6:4 v/v) followed by solvent removal using rotavapor (Buchi, Switzerland) at 40 °C. Later hydration of thin film was carried out with water at 37 °C for 2 h and subsequently it was exposed to mechanical shearing (Probe sonicator, Cole Parmer Instrument, USA) for 1 min which resulted in the formation of liposomes. Photon correlation spectroscopy (Nano ZS, Malvern UK) was used to measure the size and zeta potential of liposomal formulations. Similar method was employed for the formation of the pH sensitive DTX loaded liposomes (DTX-liposome). All the physical attributes like particle size, zeta potential and Poly Dispersity Index (PDI) were evaluated. The percentage of drug incorporation was determined by direct method [32]. Liposome dispersion was centrifuged at 40,000g for 1 h at 4 °C using an ultracentrifuge. The pellet incorporating drug was dissolved using methanol followed by estimation of the DTX concentration using a validated HPLC method [33]. For the cell culture investigations, in lieu of DTX, fluorescent dye Coumarin-6 (Cou6) was loaded in liposomes to form Cou6-liposomes [34].

### 2.2. Preparation of Lipoplex

The lipoplex were prepared using different mass ratios (lipid/shRNA). A constant amount of shRNA (2 µg) was diluted with water to a fixed volume (100 µL) in a micro-centrifuge tube. Similarly, varying volumes of liposomes at different mass ratios were taken and were diluted to 100 µL with water in different micro-centrifuge tubes. Both solutions (liposomes and shRNA) were mixed together and incubated for another 30 min at room temperature.

For comparative evaluation, Lipofectamine™2000-lipoplex and RNA-Lipoplex were also formulated by complexing shRNA with marketed transfecting agent *i.e.* Lipofectamine™2000 and pH sensitive liposomes without DTX at optimized mass ratio (similar to optimized formulation *i.e.* mass ratio 40). Likewise, for the cell culture experiments, in lieu of DTX-liposome, Cou6-liposomes were complexed with shRNA to form shRNA complexed Cou6 loaded lipoplex (Cou6-lipoplex).

Prepared shRNA complexed DTX loaded lipoplex (DTX-lipoplex) were assessed for their size and zeta potential (Nano ZS, Malvern, UK). All measurements were performed in triplicates. Surface morphology of DTX-liposome and DTX-lipoplex was assessed using Transmission Electron Microscope (TEM, FEI Tecnai™ G2 F20, U.S.A).

### 2.3. Gel retardation assay

The loading dye (2 µL, Bromophenol blue and Xylene Cyanol) was gently mixed with lipoplex (2 µL) and loaded into individual wells of agarose gel (1% w/v). Lipoplex stability was inspected before and after addition of endogenous glycosaminoglycan negative polyelectrolytes (heparin) to the pre-formed lipoplex. For heparin displacement assay, 5 µL of heparin (5000 IU/mL) was incubated with the lipoplex (20 µL) for 15 min to dissociate the complexes and then they were loaded into the wells after mixing with the loading dye. The gel was run in TAE Buffer for 45 min at 100 V followed by its visualization through UV transilluminator.

#### 2.4. pH sensitivity

The lipoplex dispersion (100  $\mu$ L) of optimized mass ratio (40, lipid/shRNA) was added to 900  $\mu$ L of ammonium acetate buffer of pH 7.4 (Physiological pH), 6.5 (Tumor microenvironment) and 5 (Tumor endosomes) separately and then it was incubated for 30 min. After the incubation period, the lipoplex were evaluated for their change in size.

#### 2.5. In vitro release

DTX release from the prepared DTX-lipoplex and DTX-liposome was evaluated by dialysis bag method. The dialysis bags (14,000 molecular weight cut off, Sigma–Aldrich, USA) containing naïve DTX and respective formulations (equivalent to 1 mg) were dispensed in 1 mL phosphate-buffered saline (PBS, 50 mM, pH 5.0, 6.5, 7.4) and then were suspended in release media (PBS, 39 mL) containing 0.5% Tween 80. Stirring for the same was done at 50 RPM (37 °C) for 48 h. At different time intervals, the aliquots of sample (~1 mL) were withdrawn and the equal volume was replaced with fresh media correspondingly. The drug content in the sample was analysed by HPLC using a reported and validated HPLC method [35].

#### 2.6. In vitro protection assays and hemocompatibility assessment

Detailed description of protection assays (in presence of DNase I and Serum) and hemocompatibility assessment along with their results is mentioned in the supplementary section.

#### 2.7. Cell culture experiments

MDA-MB-231 (human triple negative breast adenocarcinoma) and MCF-7 (human breast adenocarcinoma) cells were cultured, maintained and sub-cultured as per the ATCC guidelines. After directed trypsinization, cells were seeded in particular density in specified plates depending upon the studies (details are provided in supplementary information).

##### 2.7.1. Cell internalization studies

###### a. Qualitative cell uptake

After the attachment of the seeded MCF-7 and MDA-MB-231 (P-gp efflux sensitive) cells, culture media was aspirated and cells were washed with Hank's Buffered Salt Solution (HBSS). The cells were then exposed to free Cou6 and Cou6-lipoplex (equivalent to 1  $\mu$ g/mL of free Cou6) and were incubated for 4 h. Subsequently, cells were washed with HBSS and were fixed using paraformaldehyde (3%, Merck, India) and were observed under Confocal Laser Scanning Microscopy (CLSM, Olympus FV1000) [36].

###### b. Quantitative cell uptake

Quantitative cell uptake estimation was carried out by incubating the MCF-7 and MDA-MB-231 cells with different concentrations of various formulations (10, 15, 20  $\mu$ g/mL DTX concentrations) for several time intervals (0.5, 1, 2 and 3 h). Subsequently, cells were lysed using Triton X-100 (0.1% v/v) followed by extraction of DTX with methanol. The cell lysate was centrifuged (18,000 RPM for 10 min) and acquired supernatant was subjected to HPLC analysis for quantification of internalized DTX [37].

###### c. Inhibition studies

The confluent MCF-7 cells were pre-incubated with nontoxic concentration of the ammonium chloride (50 mM) for 25 min. Following ammonium chloride treatment, cells were exposed to Cou6-lipoplex for

2 h at 37 °C followed by analysis of the fluorescence in the cells by CLSM. Change in the fluorescence with and without the existence of ammonium chloride will help in highlighting the pH dependent cellular internalization of lipoplex [38].

###### d. Transfection efficiency

The fluorescence intensity was measured to quantify GFP expression in the transfected mammalian cells. Cultured MDA-MB-231 and MCF-7 cells were incubated with free shRNA and developed formulations (DTX-lipoplex, shRNA-lipoplex and Lipofectamine™2000-lipoplex) for 4 h in media supplemented with 10% (v/v) fetal bovine serum (FBS). After washing the cells with PBS, further incubation was carried out for up to 48 h in fresh media followed by washing. Cells were observed under CLSM at an excitation and emission wavelength corresponding to GFP (488 nm and 509 nm respectively).

For the quantification of GFP expression, washed cells were incubated with 100  $\mu$ L of lysis buffer (10 mM Tris HCl, pH 7.4, 0.5% SDS, 0.5% Triton X-100, 1 mM EDTA) and cell lysates were centrifuged to pelletize the cellular debris. Approximately 2  $\mu$ L of cell lysate was mounted on the platform of Nanodrop spectrofluorimeter (NanoDrop™ 3300, Thermo Fisher Scientific, USA) for the estimation of GFP [39].

##### 2.7.2. Cell viability

###### a. In vitro cell cytotoxicity assay

Cell cytotoxicity was performed using MTT assay MCF-7 and MDA-MB-231 cells were seeded at a density of  $10^4$  cells/well in 96-well plates and kept overnight for cell attachment. Consequently, cells were incubated with free DTX, free shRNA, shRNA-lipoplex, DTX-liposome, and DTX-lipoplex in 0.1, 1, 5 and 10  $\mu$ g/mL for 24 h. After incubation, medium containing formulation was aspirated. After washing the cells with PBS (pH 7.4), cells were processed for MTT assay as per standard protocol [33].

###### b. Apoptosis

For assessing the apoptotic potential of the formulations, MCF-7 cells were seeded in six well tissue culture plates (Costars, Corning Inc., NY, USA) and kept overnight for cell attachment [40]. The exhausted media was removed and replaced with fresh media comprising developed preparations (containing equivalent to 5  $\mu$ g/mL concentration of drug), followed by incubation for 6 h. Post incubation, the cells were washed twice with PBS and double stained with Annexin V Cy3.18 conjugate (AnnCy3) and 6-carboxyfluorescein diacetate (6-CFDA) following the manufacturer's protocol (Annexin V-Cy3™ Apoptosis Detection Kit, Sigma, USA). The cells were then visualized using CLSM under green (for 6-CFDA) and red (for AnnCy3) channels. Complete cell population can be divided into four segments depending upon the accumulated dye stained cells. Green fluorescent cells corresponded to live cells, red as necrotic, the intermediate were stained with red and green which were termed as apoptotic. The ratio of the necrotic/red fluorescence intensity to that of live/green fluorescence intensity was also assessed for the established formulations to quantify the apoptosis index.

#### 2.8. Animal studies

Animals were maintained at ambient conditions ( $25 \pm 2$  °C, RH 50–60%) having free access to food and water *ad libitum* which was kept in the plastic cages under 12 h of light/dark cycles. All the animal investigations were dually permitted by Institutional Animal Ethics Committee (IAEC) and were performed in agreement with guidelines drafted by Committee for the Purpose of Control and Supervision of Experiments on Animals (CPCSEA), India.



### 2.8.1. Antitumor efficacy

Healthy female Sprague Dawley (SD) rats (150–200 g) were used in this study. *In vivo* antitumor efficacy of the prepared formulations was explored by the reported DMBA induced animal breast cancer model [41]. Briefly, DMBA was dissolved in soya oil and was administered orally (a standard dose *i.e.* 45 mg/kg dose) to the rats in weekly intervals for 3 successive weeks. After ten weeks of last dose, all the tumor bearing animals having tumor volume above 50 mm<sup>3</sup> were segregated randomly in 7 different treatment groups each containing five animals (*n* = 5). Whereas, to follow the ethical considerations, tumor size of 100 cm<sup>2</sup> was set to be the maximum cut off limit for the selection. Single dose of each Taxotere® (Marketed DTX formulation containing DTX and high amount of surfactants to solubilise the DTX), DTX-liposome, shRNA-lipoplex, Lipofectamine™2000-lipoplex, DTX-lipoplex and free shRNA were administered intravenously (2 mg/kg of DTX) [19]. The seventh group was kept as control and was provided only normal saline in lieu of drug in similar manner. On every other day, the tumor volume was measured by measuring the tumor length (l) and width (w) using a digital calliper up to 15 days and percentage tumor reduction was calculated [42]. Finally, using Kaplan-Meier survival plot, survival of the animals was analysed to determine the mortality among groups.

### 2.8.2. Toxicity studies

#### a. Biochemical markers

Healthy female Swiss albino mice (25–30 g) were randomly divided into seven different treatment groups (*n* = 6) for the assessment of drug induced toxicities. Taxotere®, free shRNA, DTX-liposome, shRNA-lipoplex, Lipofectamine™2000-lipoplex and DTX-lipoplex (Dose equivalent of 2 mg/kg of DTX) were administered intravenously via tail vein. The last group which was kept as a control received normal saline in similar manner. Dose of DTX was adjusted and kept constant for all the formulations to maintain the optimized mass ratio and shRNA dose. After 7th day, animals were humanly sacrificed and blood was collected by cardiac puncture followed by separation of serum. Several biochemical marker (ALT, BUN and AST) levels in serum were analysed using commercially available kits [36]. All the vital organs such as liver, spleen and kidney were excised and weighed to determine the organs indices. Collected spleens were weighed for analysing the increase in the size indicating toxicity.

#### b. Renal, liver and spleen histology

Kidney, liver and spleen tissue specimens were also collected and fixed in 10% neutral buffered formalin and subjected to tissue processing followed by embedding in paraffin. The sections were further sliced into layers using microtome (Leica, Wetzlar, Germany). Hematoxylin and eosin (H&E) were used for staining them and then they were observed with microscopic examination (Olympus, Tokyo, Japan) [39].

#### c. RBC's morphology

Harvested blood was assessed for hemocompatibility using SEM imaging as reported previously in the earlier section. Any change in the morphology of RBCs was considered as toxicity markers for the formulations.

### 2.9. Statistical analysis

Statistical analysis was executed using Sigma Stat (Version 2.03) using one-way ANOVA followed by Bonferroni multiple comparison procedure. Significance was evaluated at different levels and indicated using asterisk signs as per the American Psychological Association (APA) and New England Journal of Medicine style (NEJM) of indicating *P* values.

## 3. Results

### 3.1. Preparation and optimization of liposomes

Different proportions of lipids were screened for obtaining desired physical attributes such as vesicle size and PDI. Optimized proportion of Lecithin:Cholesterol:DOTAP:DOPE (3:3:2:1) exhibited desirable size (160 ± 25 nm), zeta potential (29.43 ± 2.15 mV) and %EE (70.32 ± 5.13 at 7.5% w/w theoretical DTX loading). Prepared DTX-liposome was then subjected to complexation with shRNA for the synthesis of DTX-lipoplex. Table 1 summarises the characterization of the liposomes.

### 3.2. Preparation and characterization of lipoplex

Fig. 1(I) illustrates the particle size and surface charge (zeta potential) w.r.t different mass ratio selected for preliminary evaluation. Highest particle size of DTX-lipoplex was perceived at neutral zeta potential (mass ratio 5) owing to the minimum inter particular repulsion. Further, when the mass ratio was increased to 40 it led to the rise in zeta potential (18.47 ± 2.41 mV) which decreased the particle size *i.e.* 193.8 ± 18 nm. On the contrary, increasing trend in particle size was observed when mass ratio was increased above 40. Hence, lipoplex mass ratio of 40 was selected for further evaluations. Surface morphology assessment using TEM provided the insight of the surface attachment of the shRNA with DTX-liposome. Complexation of shRNA with the surface of DTX-liposome, changed the smoothly appearance into a rough texture (DTX-lipoplex) (Fig. 1(III)). Table 1 illustrates the changes in the physical parameters of the lipoplex after complexation of shRNA to liposomes surfaces.

#### 3.2.1. Gel retardation assay

Complexation of shRNA with liposomes was estimated using agarose gel electrophoresis. Fig. S1 demonstrates the electrophoretic mobility of liposome/shRNA complexes at different mass ratios (0.5 to 5). Complexation of liposomes with shRNA restricted the movement of the free plasmids on gel. At mass ratio 40, absolute retardation of movement was recorded indicating complete complexation of shRNA with liposomes (Fig. 1(II)). However, exposure of the heparin to DTX-lipoplex caused release of the shRNA which was then visualized as band in the gel. Intactness of the shRNA fluorescent bands and absence of smearing demonstrated the stability of shRNA in the formed lipoplex at mass ratio 40 (Fig. 1(II)).

#### 3.2.2. pH sensitivity

Incorporation of pH sensitive lipids endowed pH sensitivity to the resultant vesicles. Alteration in the surface potential and size was apparent after incubation with buffers at different pH. Fig. 2(A) demonstrated an irreversible increase in size of the lipoplex with decrease in the pH. Irreversible change might be because of the higher fusogenic nature of the lipids at the mentioned pH, leading to

**Table 1**

Changes in the physical parameters of the Lipoplex after complexation of shRNA to liposome surfaces.

| Variables                 | Parameters  |   |
|---------------------------|---|---|
|                           | pH sensitive cationic DTX-liposome (DTX-liposome) | pH sensitive cationic shRNA/DTX-lipoplex (DTX-lipoplex) |
| shRNA (μg)                | 2   | 2   |
| Volume of buffer (μL)     | 100   | 100   |
| Particles size (nm)       | 160 ± 25  | 193.8 ± 18  |
| PDI                       | 0.157 ± 0.06                                      | 0.211 ± 0.03  |
| Zeta potential (mV)       | 29.43 ± 2.15                                      | 18.47 ± 2.41  |
| DTX entrapment efficiency | 72.18 ± 3.10%                                     | 69.45 ± 1.50%   |

shRNA: Short Hairpin RNA; DTX: Docetaxel.

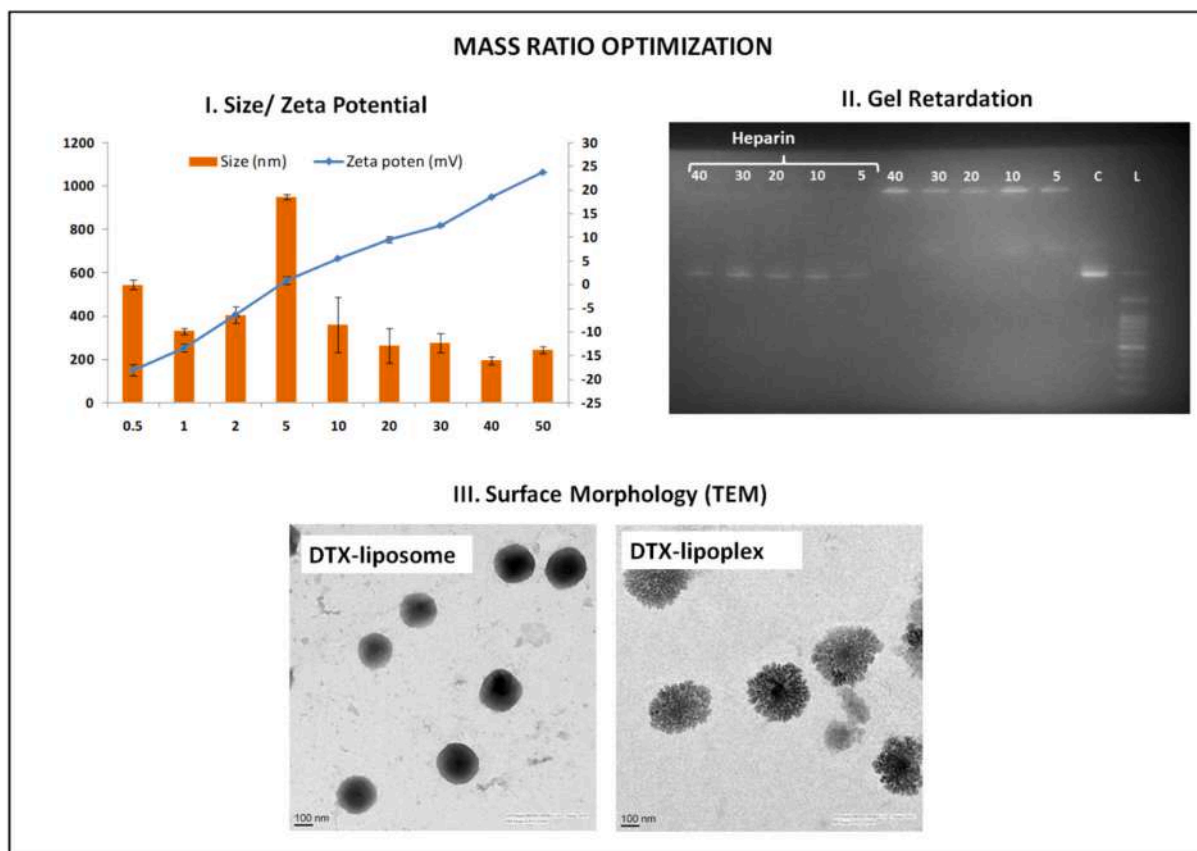


**Fig. 1.** Optimization of the DTX-lipoplex; (I) size/zeta potential with respect to mass ratio of the lipoplex; (II) gel retardation analysis/heparin displacement studies; (III) surface morphology of the DTX-liposome and DTX-lipoplex using TEM.

coagulation of the liposomes.

### 3.2.3. *In vitro* release

The cumulative release of free drug and the DTX from DTX-liposome and DTX-lipoplex is illustrated in Fig. 2(B). Within 12 h, ~99% release was evident in the case of free drug in PBS pH 7.4. It was hypothesized that DTX is not a pH-dependent drug hence, effect of pH will not be witnessed on naïve drug [43]. But the pH dependent properties of nano carriers will decide the fate of the drugs in different pH regions. Consequently, in case of pH sensitive formulations *i.e.* (DTX-liposome and DTX-lipoplex), only ~35% and ~30% release was detected respectively at pH 7.4 after 48 h. This property would increase retention time of DTX in blood circulation and will thus enhance the drug effects. Furthermore, the acid-triggered character of formulations (DTX-liposome and DTX-lipoplex) was proved by the release of drug at pH 5.0, where a consequentially elevated ( $p < 0.05$ ) cumulative release (~58%) was detected. Similarly at pH 6.5 (extravesicular tumor microenvironment), the formulation showed ~40% of release in 48 h. However, an insignificant difference ( $p > 0.05$ ) was observed between DTX-lipoplex and DTX-liposome. The studies further corroborate results of previous studies already mentioned in Section 3.2.2.

## 3.3. Cell culture experiments

### a. Cell internalization studies

Cou6-lipoplex was internalized in a better way as compared to the free Cou6 (Fig. 3(I)). Whereas, in the case of quantitative uptake estimation, the highest uptake was palpable in the case of DTX-lipoplex (~3 fold increase) followed by DTX-liposome (~2 folds increase) vis-à-vis free DTX after three hours incubation in both the cell lines (Fig. 3(II)).

Though, after three hours insignificant increment ( $p > 0.05$ ) in the uptake of lipoplex was observed which confirmed that plateau stage was reached.

### b. Inhibition study

Ammonium chloride treatment raises the pH of the late endosomes or lysosomes (acidic intracellular organelles) to inhibit endocytosis [44]. Inhibition in the uptake of Cou6-lipoplex was observed following pre-exposure with ammonium chloride. Thus, Cou6-lipoplex uptake was significantly inhibited by ammonium chloride, demonstrating the pH sensitivity to be the prominent mechanism in uptake of prepared pH sensitive lipoplex (Fig. 3(III)).

### c. Transfection efficiency

The encapsulated gene should be active enough to express in corresponding mRNA and protein after getting internalized in the cell. From the results, it is substantiated that significantly higher GFP expression ( $p < 0.001$ ) was found with DTX-lipoplex followed by Lipofectamine™2000-lipoplex and free shRNA. However, an insignificant difference ( $p > 0.05$ ) in the quantitative transfection efficiency was apparent in case of DTX-lipoplex and shRNA-lipoplex due to their inherent similar formulation characteristics (size, charge and DOPE content) (Fig. 4(I)). Consequently, a quantitative assessment of GFP expression using fluorescence spectrophotometer revealed that DTX-lipoplex exhibited 4.8, 4.5-fold appreciation (in MCF-7 and MDA-MB-231 cell lines respectively) in transfection compared to Lipofectamine™2000-lipoplex (Fig. 4(II)).

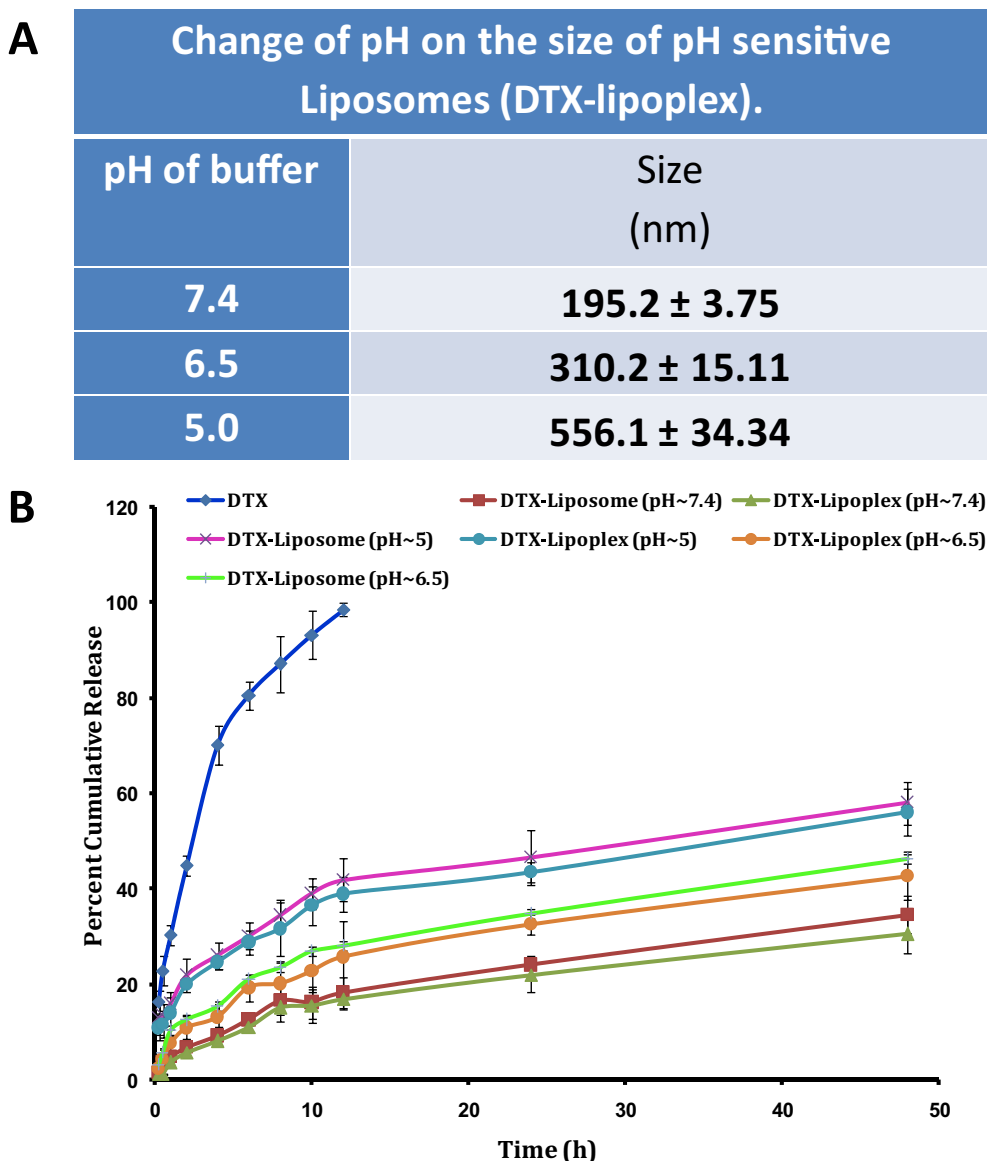


**Fig. 2.** *In vitro* investigations illustrating the pH sensitive nature of the prepared formulations. A. Tabular presentation illustrating the changes in size of the prepared formulation upon incubation in buffers at different pH; B. *in vitro* release from different formulations in various buffers at different pH.

### 3.4. Cell cytotoxicity

#### a. *In vitro* cell cytotoxicity assay

Results of MTT assay (Fig. 5(I)) clearly demonstrated that the developed formulation (DTX-lipoplex) showed notably elevated ( $p < 0.01$ ) cell toxicity in both cell lines as compared to their individual counterpart (DTX-liposome) and naive therapeutic (DTX). Fig. 5(I) illustrated the synergistic efficacy of the DTX-lipoplex by demonstrating ~2.35 and ~2.54 fold reduction in  $IC_{50}$  in comparison to DTX alone, in MDA-MB-231 and MCF-7 cells respectively. This was due to the higher internalization of corresponding formulation in cells because of their pH sensitive properties. Moreover, these findings corroborated the rational of exploring co-delivery of DTX and shRNA. Whereas, blank formulation (pH sensitive liposomes) was found to be non-toxic (Cell viability >90%, data not shown) to both the cell lines hence annulled the probability of the toxicity due to the vector itself.

#### b. Apoptosis

By coupling the action of drugs using specific genes, we can combine the stimulus to the response. Most of the cytotoxic anticancer drugs or formulations in current use have shown to induce apoptosis in susceptible cells. Results exhibited maximum apoptotic potential (1.06) with DTX-lipoplex as compared to DTX-liposome (0.82) or free DTX (0.57). Results (Fig. 5(II)) clearly indicate the collective effect of the shRNA and DTX for enhancing the apoptosis in tumor cells.

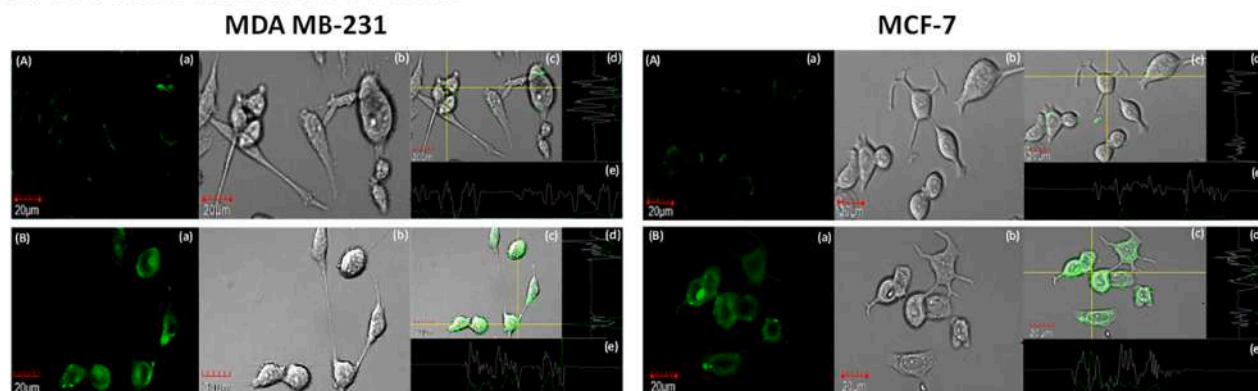
### 3.5. *In vivo* animal studies

#### 3.5.1. Antitumor activity

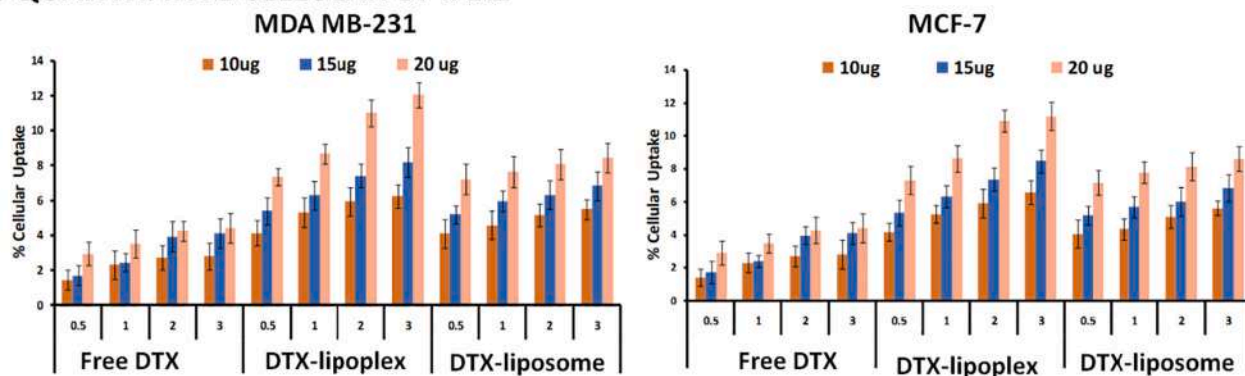
Breast tumor progressively grew reaching ~173 mm<sup>3</sup> at the end of the experiments in untreated animals (Fig. 6(A)). Following treatment with shRNA did not change the progression of breast tumor significantly, leading to an increase in the tumor mass (~162 mm<sup>3</sup>,  $P > 0.05$  as against control). However, it was found that treatment with shRNA-lipoplex slowed down the tumor growth (~35% reduction in tumor mass,  $p < 0.05$  as compared to control). Similar findings were visible in case of Lipofectamine™2000-lipoplex and Taxotere® (~31% and ~40% reduction in tumor burden respectively,  $p < 0.05$  as compared to



## I. QUALITATIVE CELLULAR UPTAKE



## II. QUANTITATIVE CELLULAR UPTAKE



## III. INHIBITION STUDIES

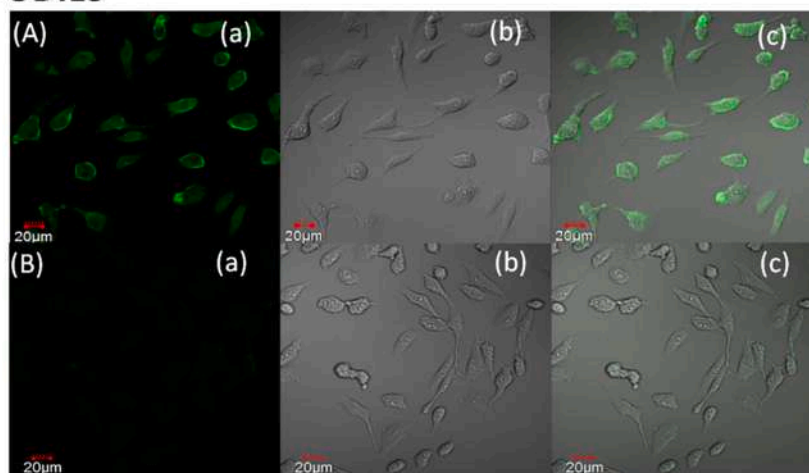


**Fig. 3.** *In vitro* cell line studies. I. Qualitative cellular uptake in MDA-MB-231 and MCF-7 cell lines: uptake of A. free dye; B. Cou6-lipoplex when incubated for 4 h (1 µg/mL). In all the images, (a) images under the green fluorescence channel; (b) corresponding differential interface contrast images of cells (c) superimposition of (a) and (b), (d) and (e) shows horizontal and vertical line series analysis of fluorescence along the white line respectively; II. quantitative cellular uptake in both the cell lines; III. inhibition assay in MDA-MB-231 cell lines, where A. uptake of Cou6-lipoplex in absence of endosome inhibition and B. uptake of Cou6-lipoplex in presence of endosome inhibitor. (For interpretation of the references to colour in this figure legend, the reader is referred to the web version of this article.)

control), but, the reduction was accompanied with the mortality of the few test animals. By encapsulating the DTX in pH sensitive liposomes (DTX-liposome), significant reduction in the tumor mass was evident (~52% reduction in tumor burden,  $p < 0.001$  in contrast to control) and also it slowed down the mortality of the animals. While DTX-lipoplex very significantly ( $P < 0.001$ ) suppressed the tumor mass (~78% reduction) as compared to control, DTX-liposome, Taxotere®, shRNA-

lipoplex or Lipofectamine™2000-lipoplex(Fig. 6(B)) alleviated the mortality in the study animals as illustrated by Kaplan Meier Survival Plot (Fig. 6(C)).

### 3.5.2. Toxicity studies

Changes in serum markers to assess the toxicity or abnormality in the blood hepato-biliary system (ALT, AST) and in the kidney (BUN,

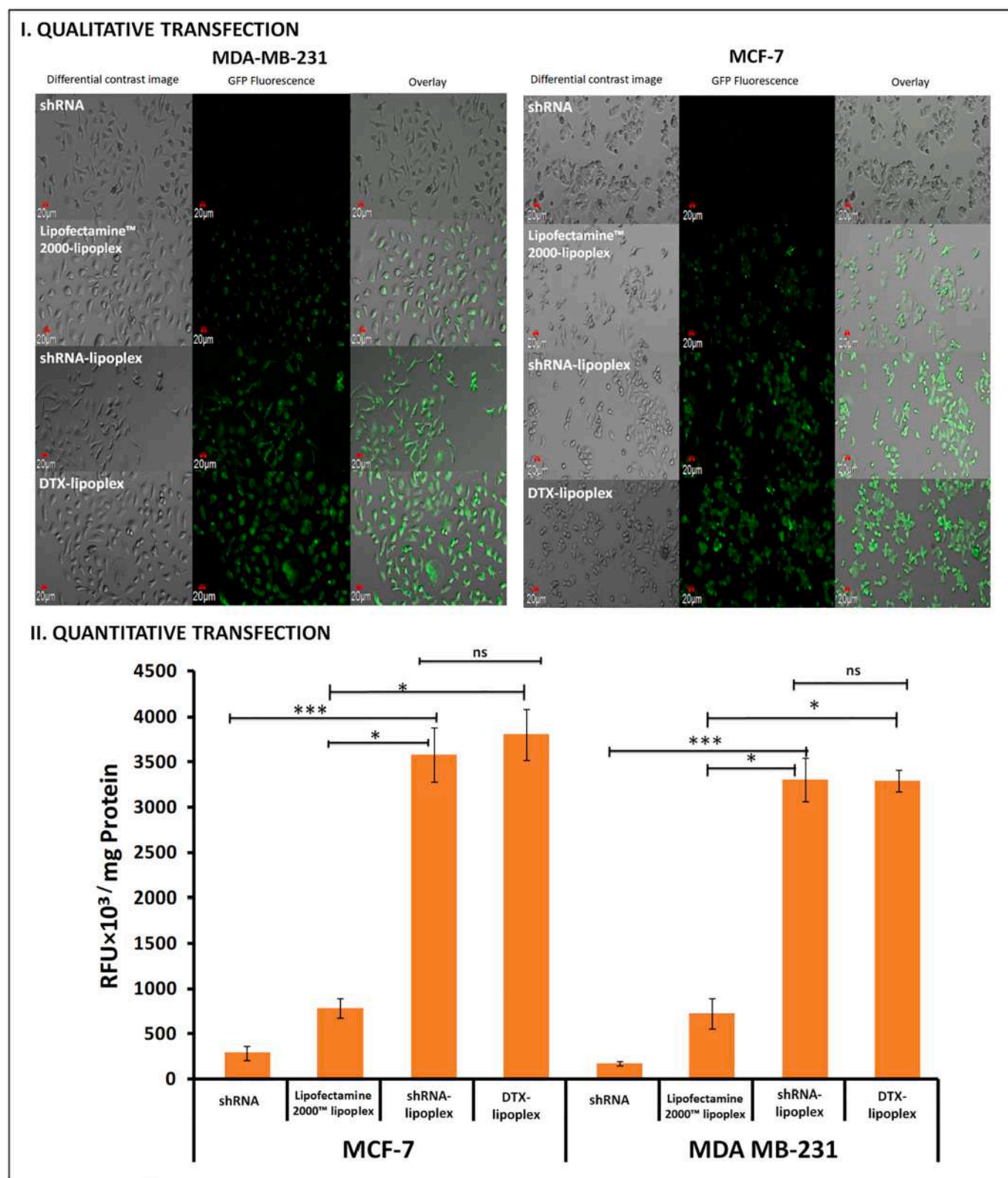


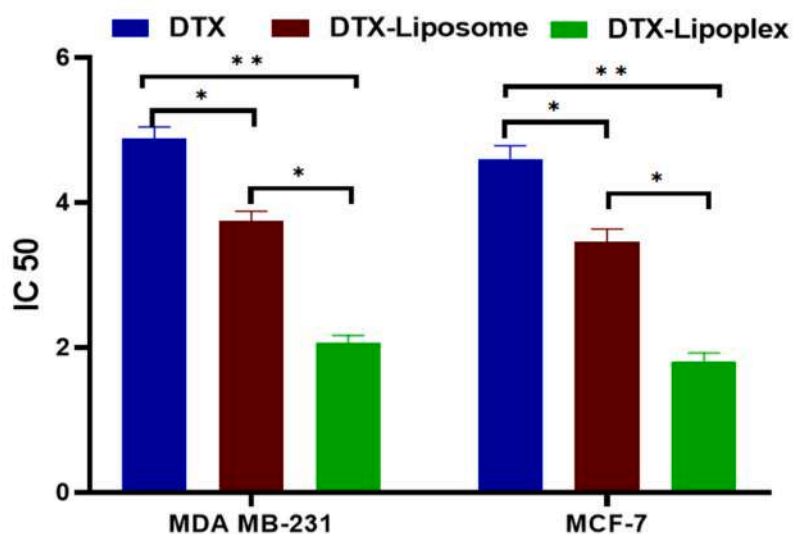
**Fig. 4.** Cell line transfection of shRNA formulations in MDA-MB-231 and MCF-7 cell lines. I. Qualitative transfection and II. quantitative transfection. Significance levels denoted as \* 0.05, \*\*  $p < 0.01$ , \*\*\*  $p < 0.001$  and ns  $p > 0.05$  (non significant).

Creatinine) illustrated significant improvement ( $p < 0.05$ ) with DTX-lipoplex (Fig. 7(A)). Significantly reduced levels of serum markers illustrated higher safety with DTX-lipoplex as compared to Lipofectamine™2000-lipoplex and Taxotere®. Histology images of the vital organs also documented less toxicity with DTX-lipoplex (Fig. 7(B)). The

histological studies of kidney, liver and spleen specimens illustrated a regular morphology in case of control group (PBS), shRNA-lipoplex and DTX-lipoplex.

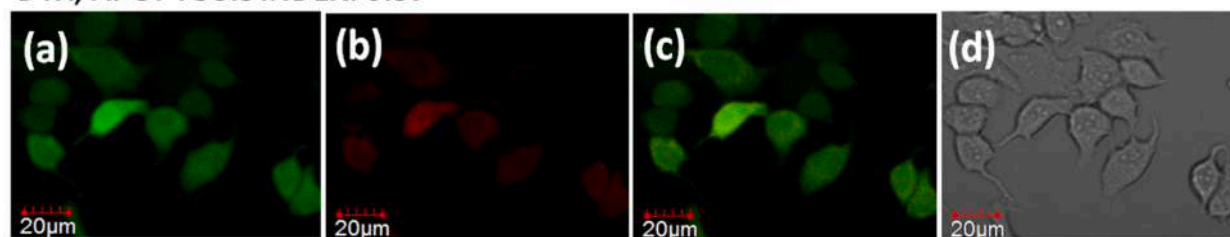
However, Taxotere® and Lipofectamine™2000-lipoplex showed toxicity to kidney (necrotic tubules and debris), liver (hepatocytes

## I. CELL CYTOTOXICITY

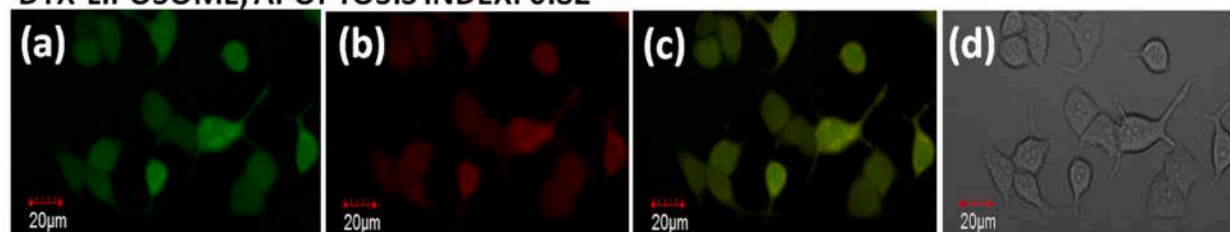


## II. APOPTOSIS ASSAY

DTX, APOPTOSIS INDEX: 0.57



DTX-LIPOSOME, APOPTOSIS INDEX: 0.82



DTX-LIPOPLEX, APOPTOSIS INDEX: 1.06

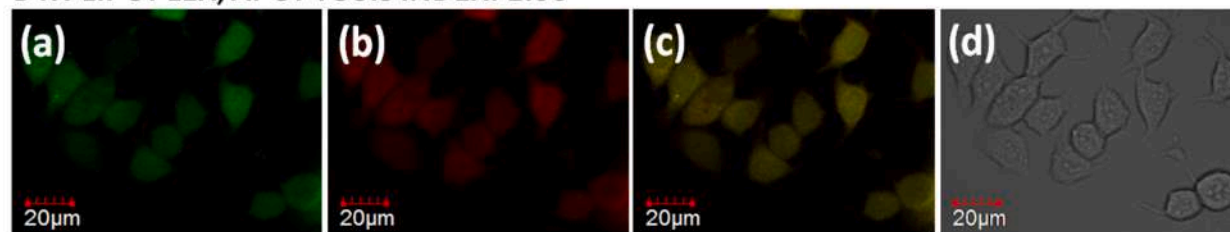


**Fig. 5.** *In vitro* cell cytotoxicity assay. I. IC<sub>50</sub> obtained from cell cytotoxicity assay; II. apoptosis assay of free DTX, DTX-liposome and DTX-lipoplex in MCF-7 cells; (a) green channel and (b) red channel depicts the fluorescence from carboxy fluorescein (cell viability marker dye) and fluorescence from Annexin Cy3.18 conjugate (cell apoptosis marker dye) respectively; (c) third channel depicts the overlay; (d) fourth represents the differential contrast image of representative cells. \* denotes  $p < 0.05$  and \*\* denotes  $p < 0.01$ . (For interpretation of the references to colour in this figure legend, the reader is referred to the web version of this article.)



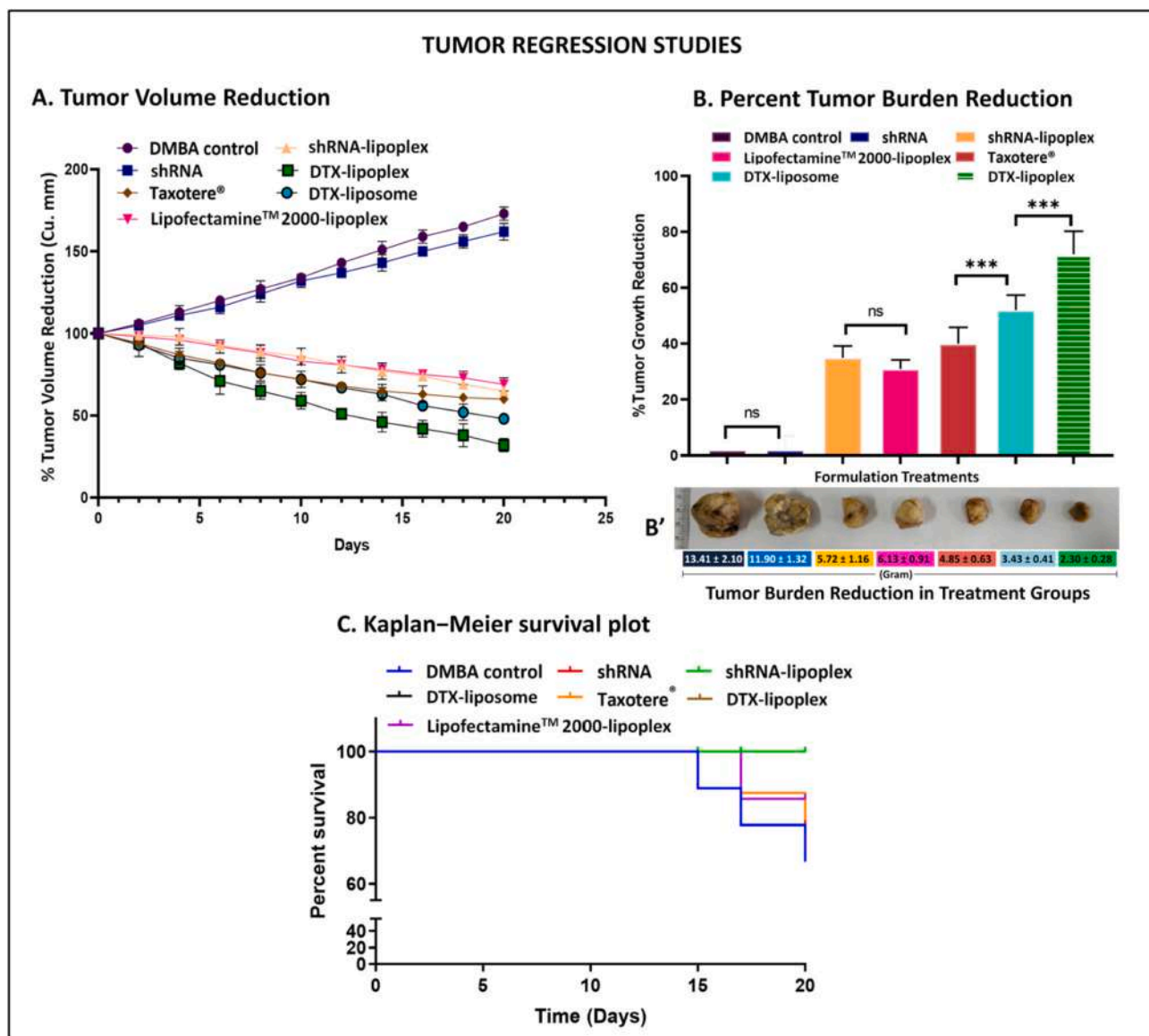


**Fig. 6.** *In vivo* animal studies. A. % Tumor volume reduction throughout the study; B. % tumor growth reduction with (B') images of the tumors isolated and weighed (grams) after terminating the tumor regression studies; C. Kaplan-Meier Survival Plot. Significance levels denoted as \* $p < 0.05$ , \*\* $p < 0.01$ , \*\*\* $p < 0.001$  and ns  $p > 0.05$  (no significance).

degeneration and infiltrations) and spleen (splenocytes damage) (Fig. 7 (B)). Increase spleen weight is another factor indicating the higher toxicity (Fig. 7(C)) in case of Taxotere®, lipofectamine™ 2000. Moreover, SEM analysis of RBCs of animals treated with Taxotere®, Lipofectamine™2000-lipoplex showed presence of many burr cells with spiked surface indicating the toxicity of the mentioned formulation to RBC's. Conversely, comparatively fewer echinocytes were visible in the case of DTX-lipoplex showing less toxicity, hence, establishing the previous toxicity results (Fig. 7(D)).

#### 4. Discussion

Designing a smart nano-vesicular system with an ability to co-deliver a bio-therapeutic molecule along with a conventional chemotherapeutic agent is what ideally desired for effective cancer management. Thus, in the current investigation, DTX loaded pH sensitive cationic liposomes (DTX-liposome) complexed with SIRT1 shRNA were prepared for establishing a better tumor management therapy. In this, pH sensitive

lipids (DOPE) were incorporated into the bilayer of liposomes which made the system environmentally sensitive towards pH change. Moreover, incorporation of cholesterol influenced the stability, fluidity, drug retention, *in vitro* release and cellular uptake of the prepared liposomes [45,46]. Furthermore, incorporation of cationic lipid (DOTAP) into the liposomal bilayer made the vesicles more fusogenic and also increased the complexation ability with the nucleic acid (cargo) [47,48].

The investigation began with the development of pH sensitive liposomes which were prepared in same way as described in our previously reported publication [26]. Then the lipoplex were examined at different mass ratios to get the desired lipoplex with minimum particle size and narrow PDI. Size of lipoplex was important as it could help in achieving better cellular internalization through the negatively charged plasma membrane along with improved stability from nucleases enzymes. Furthermore, modulation of the liposome size can also assists in increasing the circulation time [49]. Through series of examination at different mass ratio, a higher condensation with lesser size was evident with increase in mass ratio of the lipoplex. It is evident that with

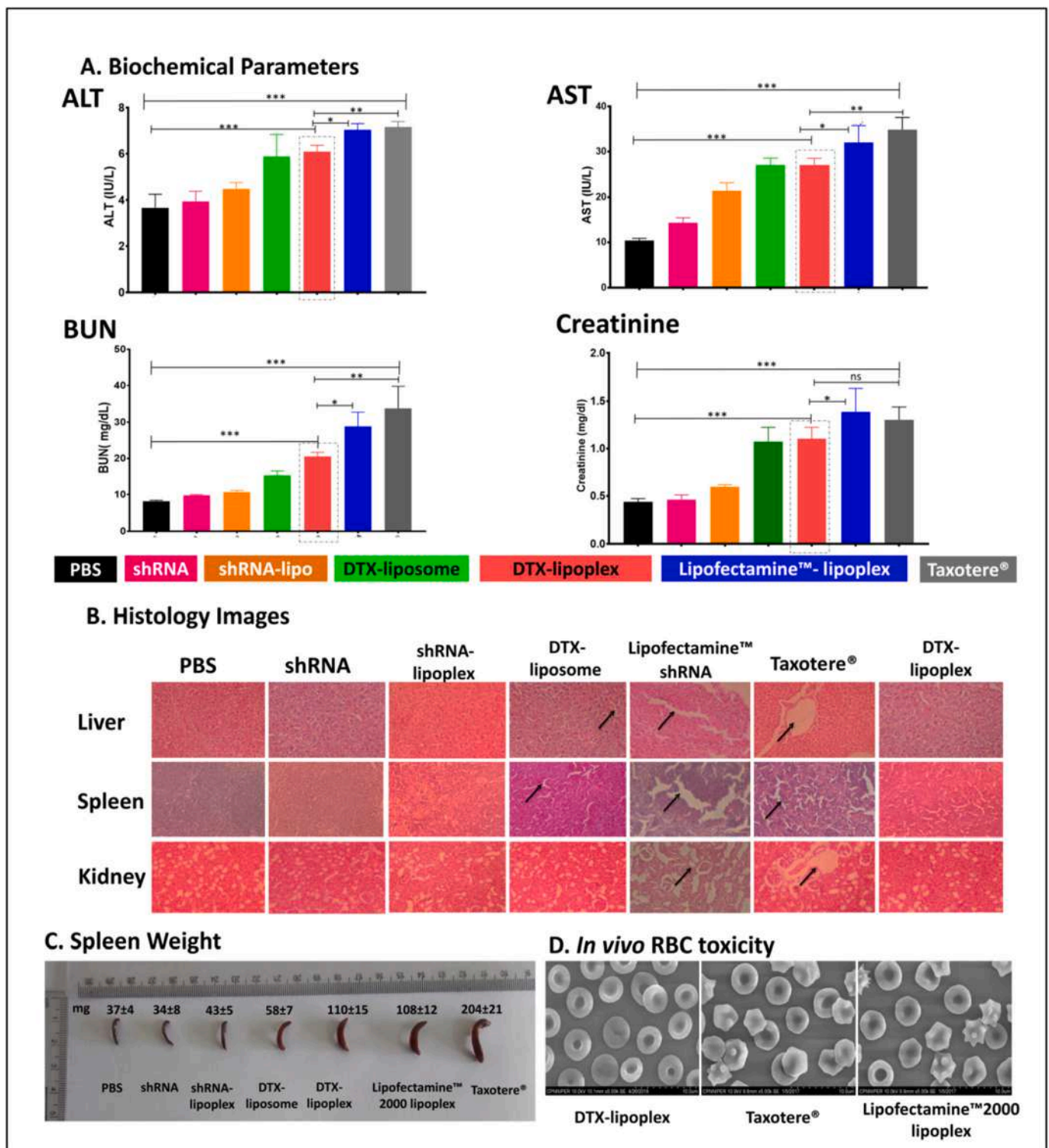


**Fig. 7.** *In vivo* toxicity evaluations using different techniques A. Biochemical parameters assessed in serum indicating changes in the hepatic and kidney biochemical parameters after 7 days treatment with formulations; B. histology Images of different vital organs such as kidney, spleen, and liver sections respectively; C. spleen weight as representation of the *in vivo* toxicity caused by formulation treatments; D. *in vivo* hemocompatibility illustrated by SEM images of RBC's. \* $p < 0.05$ , \*\* $p < 0.01$ , \*\*\* $p < 0.001$  and ns  $p > 0.05$  (no significance).

increasing mass ratio, an increase in charge of the lipoplex was observed which aids in increasing the condensation of the shRNA to liposomes. However, the increase in charge can lead to toxicity [50]. Correspondingly, mass ratio of 40 was observed to show smallest particle size with

moderately cationic zeta-potential and hence was considered ahead for further studies. One can also comment on the interaction of lipoplex by analysing the change in the zeta potential of lipoplex (~20 mV) with that of free liposomes (~30 mV) (Fig. 1(I) & Table 1). Belletti et al. also

observed a similar behaviour, stating rapid and reproducible reorganization of the shRNA around lipid material [51]. Fig. 1(II) demonstrated equidistant bands of released shRNA after treatment with heparin indicating the stability of the shRNA within the lipoplex (mass ratio 5–40). Oppositely charged heparin (anionic) destabilizes the liposome/shRNA complex by reducing the electrostatic interaction. This leads to the dissociation of liposome-shRNA complex and further sets shRNA free to move up in the electrophoretic gel. TEM images distinctively demonstrated a smooth surface for DTX-liposome, while an irregular/globular/rough surface was observed in case of DTX-lipoplex due to the shRNA complexation (Fig. 1(III)).

Further, the challenge was to evaluate whether the developed DTX-lipoplex were capable of exhibiting endosomal escape or not. Hence, change in the size of DTX-lipoplex was evaluated at pH 7.4, 6.5 and 5 (Fig. 2(A)). The mentioned pH range was selected because the ATP-dependent proton addition makes the endosomal and lysosomal compartment of the cells significantly more acidic (pH 5.0–6.2) than the tumor microenvironment (pH 6.5) or the cytoplasm (pH ~7.4). By observing the results it can be said that as pH lowers, the size of the vesicles increases, indicating the pH sensitive and fusogenic nature of the system. This is because at lower pH, DOPE exhibits a low hydration potential for its polar head group. Thus DOPE is believed to undergo a hexagonal phase inversion and form non-lamellar structures which can trigger the destabilization phenomena (endosomal pH range: pH 5–6), thereby causing a concomitant release of the encapsulated DTX and complexed shRNA in to the cytoplasm [52]. Thus, higher fusogenic ability of the developed lipoplex can assist in providing an edge over the conventional cationic liposomes. Further, to evaluate the pH sensitive effect, release studies were conducted at pH 7.4, 6.5 and 5 which also corroborated the same results (Fig. 2(B)) i.e. higher DTX was released at pH 5 than at pH 7.4.

Further, the DTX-lipoplex was evaluated for their ability to provide protection to the complexed shRNA and was tested in presence of DNase I and serum (Fig. S2(I) & (II)) using gel electrophoresis. It was observed that DTX-lipoplex formed at mass ratio of 40 can render complete protection to the complexed shRNA from DNase I for 60 min in comparison to free shRNA (Fig. S2(Ia)). The DTX-lipoplex lane showed no smearing and exhibited no extra bands which indicated that there was no DNA damage. Further, the integrity and stability of complexed shRNA was also checked by replacing it with heparin (heparin displacement assay). The preservation of solidarity of shRNA band upon replacing it with heparin in comparison to free un-treated shRNA indicated the stability of complexed shRNA within the system. The UV spectroscopy results further corroborated these findings (Fig. S2(Ib)). Similarly, no smearing or presence of additional band was observed till 4 h for DTX-lipoplex when incubated with serum (Fig. S2(II)). Hence, the ability of granting nucleases stability to the complexed shRNA is advantageous for DTX-lipoplex, as it can work as a stable shRNA pool under biological conditions. Apart from granting protection to shRNA the system must also be compatible with erythrocytes and hence, were evaluated for hemocompatibility. The surface charge and size of the vesicles as well as encapsulated drugs have a precise role to play in exhibiting hemocompatibility [53]. The hemocompatibility testing revealed an insignificant increase in the % hemolysis value for both DTX-lipoplex and Lipofectamine™2000-lipoplex (Fig. S2(III)). However, the SEM images for Lipofectamine™2000-lipoplex revealed some surface irregularities. We reasoned that it was due to the higher surface cationic charge of Lipofectamine™2000 in comparison to DTX-lipoplex. Thus, it can be said that the DTX-lipoplex are hemocompatible with notably less erythrocyte interaction.

The higher fusogenic ability of the developed lipoplex can provide an added advantage over the conventional liposomes and to test that, cell internalization studies were performed. A significantly higher uptake for the Cou6 loaded lipoplex was visible in comparison to Cou6 dye alone in both the cell lines (i.e. MDA-MB-231 and MCF-7) (Fig. 3(I)). Similarly, DTX-lipoplex revealed ~3 fold higher drug titer within the cells as

compared to their naïve group (Fig. 3(II)). This higher cellular uptake could be due to the cationic surface and pH sensitive nature of the liposomes. We also argue that the presence of DOPE is crucial for exhibiting higher cellular uptake as; it is a prominent element to show endosomal disruption and exhibiting the release of content into the cytoplasm. That explains similar responses in case of all the pH-sensitive cationic lipidic formulations. To understand the pH responsive uptake mechanism, cells were pre-incubated with lysosomal inhibitors (Ammonium Chloride) to constrain the pH change and subsequently inhibiting the uptake of the formulations. Exposure of lysosomal inhibitors inhibits endocytosis by raising the pH of acidic endosomes which can therefore make DOPE ineffective (Fig. 3(III)). The reduction in the uptake of the Cou6 loaded lipoplex after the lysosomal inhibitor treatment corroborated the results obtained with previous *in vitro* pH studies. This also substantiated the cell uptake enhancer role of DOPE.

Furthermore, the developed lipoplex were evaluated for their capability of providing an easy and safe passage to the complexed shRNA (carrying GFP sequence) in to the cancer cells. This was verified by assessing the expression of GFP in targeted cells (Fig. 4). DTX-lipoplex showed higher transfection as compared to the fragile and unstable free shRNA. However, an insignificant difference ( $p > 0.05$ ) in GFP expression among shRNA-lipoplex and DTX-lipoplex was observed in both the cell lines. This might be due to the similar native physico-chemical characteristics such as surface potential, size, and pH sensitivity. However, both formulations showed a significantly higher ( $p < 0.001$ ) transfection as compared to marketed counterpart (Lipofectamine™2000-lipoplex) due to their pH sensitive nature. As, it was evident from the cellular internalization studies that DTX-lipoplex was capable of exhibiting higher DTX titre in to the cancer cells, this led the system to exhibit higher cellular cytotoxicity in both the cell lines. This increased retention of intracellular drug concentration could have been attributed due to the action of co-delivered shRNA which might have assisted in exerting an augmented efficacy as evident by the multiple fold decrease in cell viability (lower IC<sub>50</sub> of the developed formulations, Fig. 5(I)). The increased potency of the therapy was further substantiated by apoptosis studies (Fig. 5(II)). However, higher effects of DTX-liposome than free DTX could be due to the pH sensitivity and higher positive surface of the liposomes.

The SIRT1 gene was identified to exert a vital role in context of oncogenic signalling in progression of the breast cancer [54]. Similarly, previous reports also substantiated through *in vivo* investigations that invasive aptitude of SIRT1 was notably abridged by retardation of SIRT1 gene in human TNBC cell lines [55]. Depicted hypothesis and substantial *in vitro* data inspired us to undertake *in vivo* tumor regression studies. *In vivo* results authenticated the significant and combinational potential of the developed DTX-lipoplex in reducing the tumor burden as compared to their counterparts (shRNA, shRNA-lipoplex, DTX-liposome and their marketed alternative i.e. Taxotere®, Lipofectamine™2000-lipoplex) (Fig. 6). Hence, it can be concluded that co-delivery systems mitigate the tumor condition by concurrently obstructing SIRT1 governed pathways and making the cells sensitive towards death signals. However, further studies are required to confirm and authenticate these facts.

The biochemical parameters in case DTX-lipoplex were found to be significantly reduced as compared to marketed formulations (Taxotere® and Lipofectamine™2000-lipoplex) (Fig. 7(A)). It was encouraging that the *in vivo* biocompatibility and toxicity studies did not show any signs of hepatic, renal or spleen toxicity after intravenous injection of the nano vesicles. Developed formulations illustrated a significantly reduced hepatotoxicity and nephrotoxicity as compared to the marketed formulation (Taxotere®) (Fig. 7(B)). Localized pH responsive tumor delivery, reduced leakage of the drug in systematic circulation and prolongation of circulation time might have worked in harmony for decreasing the exposure of drugs to normal tissues [56,57]. Further, the toxic effect caused by the harsh adjuvant (Tween® 80) used in Taxotere® can also be avoided in the present developed formulation [29].

Likewise, Kaplan–Meier survival analysis (Fig. 6(C)) also illustrated



the overall reduced toxicity of the developed formulation w.r.t. marketed formulation. Tested formulations may cause many incompatibilities to the erythrocytes *in vivo*. The *in vivo* RBC toxicity was also assessed in different groups. SEM images clearly depicted that DTX-lipoplex showed significantly fewer erythrocyte surface alterations (Echinocyte) as compared to marketed formulations (Taxotere® and Lipofectamine™2000-lipoplex) (Fig. 7(D)). These results were found to be in line with the *in vitro* haemolytic assay.

Due to increased cell proliferation and inadequate angiogenesis, the clustered tumor vessels remain undeveloped and hyper-permeable. As a result, therapeutic particles (<200 nm) would direct specifically to tumor and will not extravasate to normal tissues (reduce adverse effect) due to the enhanced permeation and retention (EPR) effect. The effect was further aggravated by the pH sensitive nature of the lipoplex due to incorporated lipids (DOPE). Our previous published report highlights the significance of pH sensitive cationic liposomes manoeuvring EPR effect [25]. Moreover current publication potentially illustrates that, the passive targeting, co-delivery (DTX and shRNA), ease in release cargo in the tumor cells and decreased toxicity, account for the superiority of DTX-lipoplex over other formulations. Cumulatively, the data suggested a higher efficiency of DTX-lipoplex in the management and treatment of breast tumor.

## 5. Conclusion

Potentiating the existing therapy by combining the advantages of the two types of therapeutics (biological and chemotherapeutics) will heighten the response of the therapy. This intensified response could be either obtained from the knocking down the oncogenic gene, arresting the cell cycle, sensitising the cells to drug response or raising the drug titre in the cancer cells. In the present investigation, mentioned approaches were utilized to augment the effectiveness of the therapy by coupling it with pH sensitive cytosolic tumor specific liposomes. Though, it is very much necessary to understand the mechanistic cascade to appreciate the established results. However, it can precisely be concluded that co-delivering biological and chemotherapeutic therapeutics in a single tumor-specific nanopatform will help to improve the effective therapeutic potential of the current therapy and will help to save cancer patients, who are in clinical needs of innovative solutions.

## Declaration of competing interest

The authors have no relevant affiliation financial involvement with any organization or entity with financial interest with the subject of the matter disclosed in the manuscript. The authors declare no conflict of interest.

## Acknowledgement

RS is grateful to Science and Engineering Research Board (SERB), DST, GOI, New Delhi, for providing research fellowship. Authors are also thankful to Mr. Rahul Mahajan, NIPER, S.A.S. Nagar for his technical assistance.

## Funding sources

None.

## Ethical conduct of research statement

All the animal studies protocols were duly approved by the Institutional Animal Ethics Committee (IAEC), NIPER, India.

## CRedit authorship contribution statement

**Rajan Swami:** (Conceptualization, Methodology, Validation, Formal

analysis, Investigation, Resources, Writing - Original Draft, Writing - Review & Editing, Visualization and Project administration).

**Yogesh Kumar:** (Methodology, Validation, Formal analysis, Investigation, Data curation and Visualization).

**Dasharath Chaudhari:** (Conceptualization, Methodology, Validation, Project administration).

**Sameer S. Katiyar:** (Conceptualization, Validation, Formal analysis and Project administration).

**Kaushik Kuche:** (Resources, Writing - Original Draft, Writing - Review & Editing and Visualization).

**Parmeshwar B. Katore:** (Conceptualization, Resources, Data curation, and Project administration).

**Sanjay K. Banerjee:** (Conceptualization, Resources, Data curation, Supervision and Project administration).

**Sanyog Jain:** (Conceptualization, Methodology, Validation, Formal analysis, Investigation, Resources, Data curation, Writing - Review & Editing, Visualization, Supervision and Project administration).

## Appendix A. Supplementary data

Supplementary data to this article can be found online at <https://doi.org/10.1016/j.msec.2020.111664>.

## References

- [1] B. Mansoori, S.S. Shotorbani, B. Baradaran, RNA interference and its role in cancer therapy, *Adv. Pharm. Bull.* 4 (2014) 313.
- [2] Z. Wang, D.D. Rao, N. Senzer, J. Nemunaitis, RNA interference and cancer therapy, *P. Pharm. Res.* 28 (2011) 2983–2995.
- [3] R.B. Mokhtari, T.S. Homayouni, N. Baluch, E. Morgatskaya, S. Kumar, B. Das, H. Yeger, Combination therapy in combating cancer, *Oncotarget* 8 (2017) 38022.
- [4] C. Feng, J. Ouyang, Z. Tang, N. Kong, Y. Liu, L. Fu, X. Ji, T. Xie, O.C. Farokhzad, W. Tao, Germanene-based theranostic materials for surgical adjuvant treatment: inhibiting tumor recurrence and wound infection, *Matter* 3 (2020) 127–144.
- [5] K.K. Hunt, S.A. Vorbuerger, Hurdles and hopes for cancer treatment, *Sci.* 297 (2002) 415–416.
- [6] R. Swami, I. Singh, W. Khan, S. Ramakrishna, Diseases originate and terminate by genes: unravelling nonviral gene delivery, *Drug Deliv. Transl. Rev.* 3 (2013) 593–610.
- [7] N. Amreddy, A. Babu, R. Muralidharan, J. Panneerselvam, A. Srivastava, R. Ahmed, M. Mehta, A. Munshi, R. Ramesh, Recent advances in nanoparticle-based cancer drug and gene delivery, in: *Advances in Cancer Research*, Elsevier, 2018, pp. 115–170.
- [8] N. Kong, W. Tao, X. Ling, J. Wang, Y. Xiao, S. Shi, X. Ji, A. Shajii, S.T. Gan, N.Y. Kim, Synthetic mRNA nanoparticle-mediated restoration of p53 tumor suppressor sensitizes p53-deficient cancers to mTOR inhibition, *Sci. Transl. Med.* 11 (2019).
- [9] M.A. McAnuff, G.R. Rettig, K.G. Rice, Potency of siRNA versus shRNA mediated knockdown *in vivo*, *J. Pharm. Sci.* 96 (2007) 2922–2930.
- [10] D.D. Rao, J.S. Vorhies, N. Senzer, J. Nemunaitis, siRNA vs. shRNA: similarities and differences, *Adv. Drug Deliv. Rev.* 61 (2009) 746–759.
- [11] A.M. Chen, M. Zhang, D. Wei, D. Stueber, O. Taratula, T. Minko, H. He, Co-delivery of doxorubicin and Bcl-2 siRNA by mesoporous silica nanoparticles enhances the efficacy of chemotherapy in multidrug-resistant cancer cells, *Small* 5 (2009) 2673–2677.
- [12] Y. Ren, C.-S. Kang, X.-B. Yuan, X. Zhou, P. Xu, L. Han, G.X. Wang, Z. Jia, Y. Zhong, S. Yu, Co-delivery of as-miR-21 and 5-FU by poly (amidoamine) dendrimer attenuates human glioma cell growth *in vitro*, *J. Biomater. Sci. Polym. Ed.* 21 (2010) 303–314.
- [13] M. Saad, O.B. Garbuzenko, T. Minko, Co-delivery of siRNA and an anticancer drug for treatment of multidrug-resistant cancer, *Nanomed.* 3 (2008) 761–776.
- [14] G. Shim, S.-E. Han, Y.-H. Yu, S. Lee, H.Y. Lee, K. Kim, I.C. Kwon, T.G. Park, Y. B. Kim, Y.S. Choi, Trilysinoyleylamide-based cationic liposomes for systemic co-delivery of siRNA and an anticancer drug, *J. Control. Release* 155 (2011) 60–66.
- [15] A. Schulte, K. Liffers, A. Kathagen, S. Riethdorf, S. Zapf, A. Merlo, K. Kolbe, M. Westphal, K. Lamszus, Erlotinib resistance in EGFR-amplified glioblastoma cells is associated with upregulation of EGFRvIII and PI3Kp110 $\delta$ , *Neuro-oncology* 15 (2013) 1289–1301.
- [16] E. Alton, M. Stern, R. Farley, A. Jaffe, S. Chadwick, J. Phillips, J. Davies, S. Smith, J. Browning, M. Davies, Cationic lipid-mediated CFTR gene transfer to the lungs and nose of patients with cystic fibrosis: a double-blind placebo-controlled trial, *Lancet* 353 (1999) 947–954.
- [17] V.P. Torchilin, Cell penetrating peptide-modified pharmaceutical nanocarriers for intracellular drug and gene delivery, *J. Pept. Sci.* 90 (2008) 604–610.
- [18] J. Jiang, S.-j. Yang, J.-c. Wang, L.-j. Xu, T. Yang, X.-y. Liu, Q. Zhang, Sequential treatment of drug-resistant tumors with RGD-modified liposomes containing siRNA or doxorubicin, *Eur. J. Pharm. Biopharm.* 76 (2010) 170–178.
- [19] T. Yang, B. Li, S. Qi, Y. Liu, Y. Gai, P. Ye, G. Yang, W. Zhang, P. Zhang, X. He, Co-delivery of doxorubicin and Bmi1 siRNA by folate receptor targeted liposomes

- exhibits enhanced anti-tumor effects in vitro and in vivo, *Theranostics* 4 (2014) 1096.
- [20] W. Xiao, X. Chen, L. Yang, Y. Mao, Y. Wei, L. Chen, Co-delivery of doxorubicin and plasmid by a novel FGFR-mediated cationic liposome, *Int. J. Pharm.* 393 (2010) 120–127.
- [21] H.R. Oh, H.-Y. Jo, J.S. Park, D.-E. Kim, J.-Y. Cho, P.-H. Kim, K.-S. Kim, Galactosylated liposomes for targeted co-delivery of doxorubicin/vimentin siRNA to hepatocellular carcinoma, *J. Nanomater.* 6 (2016) 141.
- [22] X. Ji, Y. Kang, J. Ouyang, Y. Chen, D. Artzi, X. Zeng, Y. Xiao, C. Feng, B. Qi, N. Y. Kim, Synthesis of ultrathin biotite nanosheets as an intelligent theranostic platform for combination cancer therapy, *Adv. Sci.* 6 (2019) 1901211.
- [23] W. Tao, J. Wang, W.J. Parak, O.C. Farokhzad, J. Shi, Nanobuffering of pH-responsive polymers: a known but sometimes overlooked phenomenon and its biological applications, *ACS Nano* 13 (2019) 4876–4882.
- [24] J.-Y. Legendre, F.C. Szoka Jr, Delivery of plasmid DNA into mammalian cell lines using pH-sensitive liposomes: comparison with cationic liposomes, *Pharm. Res.* 9 (1992) 1235–1242.
- [25] Y. Kumar, K. Kuche, R. Swami, S.S. Katiyar, D. Chaudhari, P.B. Katare, S. K. Banerjee, S. Jain, Exploring the potential of novel pH sensitive lipoplexes for tumor targeted gene delivery with reduced toxicity, *Int. J. Pharm.* 573 (2020) 118889.
- [26] E.-J. Kim, S.-J. Um, SIRT1: roles in aging and cancer, *BMB Rep.* 41 (2008) 751–756.
- [27] Z. Wang, W. Chen, Emerging roles of SIRT1 in cancer drug resistance, *Genes & Cancer* 4 (2013) 82–90.
- [28] X. Jin, Y. Wei, F. Xu, M. Zhao, K. Dai, R. Shen, S. Yang, N. Zhang, SIRT1 promotes formation of breast cancer through modulating Akt activity, *J. Cancer* 9 (2018) 2012.
- [29] L.S. Schwartzberg, R.M. Navari, Safety of polysorbate 80 in the oncology setting, *Adv. Ther.* 35 (2018) 754–767.
- [30] L. Kaushik, S. Srivastava, A. Panjeta, D. Chaudhari, R. Ghadi, K. Kuche, R. Malik, S. Preet, S. Jain, K. Raza, Exploration of docetaxel palmitate and its solid lipid nanoparticles as a novel option for alleviating the rising concern of multi-drug resistance, *Int. J. Pharm.* 578 (2020) 119088.
- [31] J. Crown, M. O'Leary, W.S. Ooi, Docetaxel and paclitaxel in the treatment of breast cancer: a review of clinical experience, *Oncologist* 9 (2004) 24–32.
- [32] S. Jain, D. Kumar, N.K. Swarnakar, K. Thanki, Polyelectrolyte stabilized multilayered liposomes for oral delivery of paclitaxel, *Biomaterials* 33 (2012) 6758–6768.
- [33] R. Swami, I. Singh, M.K. Jeengar, V. Naidu, W. Khan, R. Sistla, Adenosine conjugated lipidic nanoparticles for enhanced tumor targeting, *Int. J. Pharm.* 486 (2015) 287–296.
- [34] S. Jain, D.P. Kale, R. Swami, S.S. Katiyar, Codelivery of benzoyl peroxide & adapalene using modified liposomal gel for improved acne therapy, *Nanomed.* 13 (2018) 1481–1493.
- [35] J. Zhang, C. Yang, S. Pan, M. Shi, J. Li, H. Hu, M. Qiao, D. Chen, X. Zhao, Eph A10-modified pH-sensitive liposomes loaded with novel triphenylphosphine-docetaxel conjugate possess hierarchical targetability and sufficient antitumor effect both in vitro and in vivo, *Drug Deliv.* 25 (2018) 723–737.
- [36] S. Jain, G. Spandana, A.K. Agrawal, V. Kushwah, K. Thanki, Enhanced antitumor efficacy and reduced toxicity of docetaxel loaded estradiol functionalized stealth polymeric nanoparticles, *Mol. Pharm.* 12 (2015) 3871–3884.
- [37] A.K. Jain, K. Thanki, S. Jain, Co-encapsulation of tamoxifen and quercetin in polymeric nanoparticles: implications on oral bioavailability, antitumor efficacy, and drug-induced toxicity, *Mol. Pharm.* 10 (2013) 3459–3474.
- [38] O.P. Perumal, R. Inapagolla, S. Kannan, R.M. Kannan, The effect of surface functionality on cellular trafficking of dendrimers, *Biomaterials* 29 (2008) 3469–3476.
- [39] H. Mandal, S.S. Katiyar, R. Swami, V. Kushwah, P.B. Katare, A.K. Meka, S.K. Banerjee, A. Popat, S. Jain,  $\epsilon$ -Poly-L-lysine/plasmid DNA nanoplexes for efficient gene delivery in vivo, *Int. J. Pharm.* 542 (2018) 142–152.
- [40] C.P. Dora, V. Kushwah, S.S. Katiyar, P. Kumar, V. Pillay, S. Suresh, S. Jain, Improved oral bioavailability and therapeutic efficacy of erlotinib through molecular complexation with phospholipid, *Int. J. Pharm.* 534 (2017) 1–13.
- [41] J.P. Desale, R. Swami, V. Kushwah, S.S. Katiyar, S. Jain, Chemosensitizer and docetaxel-loaded albumin nanoparticle: overcoming drug resistance and improving therapeutic efficacy, *Nanomed.* 13 (2018) 2759–2776.
- [42] A.K. Jain, K. Thanki, S. Jain, Co-encapsulation of tamoxifen and quercetin in polymeric nanoparticles: implications on oral bioavailability, antitumor efficacy, and drug-induced toxicity, *Mol. Pharm.* 10 (2013) 3459–3474.
- [43] J.-S. Choi, J.-S. Park, Development of docetaxel nanocrystals surface modified with transferrin for tumor targeting, *Drug Des. Devel.* 11 (2017) 17.
- [44] S. Simões, J.N. Moreira, C. Fonseca, N. Düzgüneş, M.C.P. de Lima, On the formulation of pH-sensitive liposomes with long circulation times, *Adv. Drug Deliv. Rev.* 56 (2004) 947–965.
- [45] A.K. Katragadda, M. Singh, G.V. Betageri, Encapsulation, stability, and in vitro release characteristics of liposomal formulations of stavudine (D4T), *Drug Deliv.* 6 (1999) 31–37.
- [46] Y.-U. Bae, J.-W. Huh, B.-K. Kim, H.Y. Park, Y.-B. Seu, K.-O. Doh, Enhancement of liposome mediated gene transfer by adding cholesterol and cholesterol modulating drugs, *BBA-Biomembranes* 1858 (2016) 3017–3023.
- [47] B.-K. Kim, G.-B. Hwang, Y.-B. Seu, J.-S. Choi, K.S. Jin, K.-O. Doh, DOTAP/DOPE ratio and cell type determine transfection efficiency with DOTAP-liposomes, *BBA-Biomembranes* 1848 (2015) 1996–2001.
- [48] K. Stebelska, P. Wyrozumska, J. Gubernator, A.F. Sikorski, Highly fusogenic cationic liposomes transiently permeabilize the plasma membrane of HeLa cells, *Cell. Mol. Biol. Lett.* 12 (2007) 39–50.
- [49] M. Çağdaş, A.D. Sezer, S. Bucak, Liposomes as potential drug carrier systems for drug delivery, in: *Application of Nanotechnology in Drug Delivery*, 2014.
- [50] M. Brgles, M. Santak, B. Halassy, D. Forcic, J. Tomašić, Influence of charge ratio of liposome/DNA complexes on their size after extrusion and transfection efficiency, *Int. J. Nanomedicine* 7 (2012) 393.
- [51] D. Belletti, M. Tonelli, F. Forni, G. Tosi, M.A. Vandelli, B. Ruozzi, AFM and TEM characterization of siRNA lipoplexes: a combinatory tools to predict the efficacy of complexation, *Colloid. Surface. A* 436 (2013) 459–466.
- [52] G. Moku, S.K. Gulla, N.V. Nimmu, S. Khalid, A. Chaudhuri, Delivering anti-cancer drugs with endosomal pH-sensitive anti-cancer liposomes, *Biomater. Sci.* 4 (2016) 627–638.
- [53] L. Chen, J.D. Simpson, A.V. Fuchs, B.E. Rolfe, K.J. Thurecht, Effects of surface charge of hyperbranched polymers on cytotoxicity, dynamic cellular uptake and localization, hemotoxicity, and pharmacokinetics in mice, *Mol. Pharm.* 14 (2017) 4485–4497.
- [54] M.F. Santolla, S. Avino, M. Pellegrino, E. De Francesco, P. De Marco, R. Lappano, A. Vivacqua, F. Cirillo, D. Rigracchio, A. Scarpelli, SIRT1 is involved in oncogenic signaling mediated by GPER in breast cancer, *Cell Death Dis.* 6 (2015) e1834.
- [55] S.Y. Chung, Y.Y. Jung, I.A. Park, H. Kim, Y.R. Chung, J.Y. Kim, S.Y. Park, S.-A. Im, K.-H. Lee, H.-G. Moon, Oncogenic role of SIRT1 associated with tumor invasion, lymph node metastasis, and poor disease-free survival in triple negative breast cancer, *Clin. Exp. Metastasis* 33 (2016) 179–185.
- [56] O.V. Gerasimov, J.A. Boomer, M.M. Qualls, D.H. Thompson, Cytosolic drug delivery using pH- and light-sensitive liposomes, *Adv. Drug Deliv. Rev.* 38 (1999) 317–338.
- [57] Y. Lv, L. Hao, W. Hu, Y. Ran, Y. Bai, L. Zhang, Novel multifunctional pH-sensitive nanoparticles loaded into microbubbles as drug delivery vehicles for enhanced tumor targeting, *Sci. Rep.* 6 (2016) 29321.